Subtle Structural Distortions in Some Dielectric Perovskites

Rajeev Ranjan

Abstract | Dielectric perovskites exhibit a range of interesting phenomenon such as ferroelectricity, piezoelectricity, pyroelectricity, which have important technological implications. These materials show strong structure–property correlations. Majority of the perovskites exhibit crystal structures, which can be described in terms of distortions of the cubic prototype. In some cases the distortions are extremely weak and impossible to detect by x-ray diffraction (even at synchrotron sources). In such cases, use of complementary techniques, such as neutron powder diffraction and electron microdiffraction, are mandatory to reveal them. This paper reviews the work we have carried out over the past one decade on some dielectric and ferroelectric perovskites, with special emphasis on the subtle aspects of the structural distortions. Examples are taken from systems such as $SrTiO_3$–$CaTiO_3$, $PbZrO_3$–$PbTiO_3$, $Na_{0.5}Ln_{0.5}TiO_3$ (Ln = La, Pr and Nd), $Na_{0.5}Nd_{0.5}TiO_3$–$SrTiO_3$ and Pr-doped $SrTiO_3$. The first four cases have been chosen to highlight the global symmetry breaking due to the subtle distortions, some of them of very uncommon type. The last example emphasizes how analysis of the anomalous value of lattice parameter obtained by Rietveld refinement of the cubic structure is linked with the development of ferroelectric polar nano regions in the system.

1. Introduction

The perovskite structure type is one of the most frequently encountered in materials science. Historically, the word "perovskite" was first coined in 1839 by a Russian mineralogist, Rose, who discovered the mineral $CaTiO_3$ and gave it the name "Perovskite" in honour of the then minister of Lands, L. A. Perovsky. In later years, this term became a representative of a family of a large number of ABX_3 compounds. Perovskites exhibit wide ranging physical phenomena, and continue to throw up ever surprising properties from time to time. Among the interesting phenomena include the ferroelectricity in $BaTiO_3$[1–3] piezoelectricity in $Pb(Zr_{1-x}Ti_x)O_3$[3–5], superconductivity in $BaBiO_3$[6], colossal magnetoresistance in doped manganites $Ln_{1-x}A_xO_3$ (Ln = lanthanide ion, A = alkaline earth ion)[7], quantum paraelectricity[8], Jahn Teller transitions in $LaMnO_3$[7], and magnetoelectric-multiferroicity $BiMnO_3$ and $BiFeO_3$[9,10]. The ensuing properties arising out of some of these phenomena give rise to important actual and potential applications. For example, $BaTiO_3$, due to its large dielectric constant at room temperature, is one of the major constituent of multilayer ceramic capacitors[3]. These capacitors contribute significantly to the miniaturization of electronic products and are being used in notebook computers and mobile phones. $BaTiO_3$ is also used for thermistor devices[3]. A huge industry is based on the high performance sensing and actuation properties of lead-zirconate-titanate ($PbZrO_3$–$PbTiO_3$), famously known as PZT[3,4]. A close relative of perovskite, WO_3, finds application in electrochromic windows. With the expansion of satellite based communications and broadcasting,

Department of Materials Engineering, Indian Institute of Science, Bangalore 560012, India
rajeev@materials.iisc.ernet.in

Figure 1: A cubic ABO_3perovskite structure. The B cations are at the centre of the octahedra and the A cation is located between the octahedra.

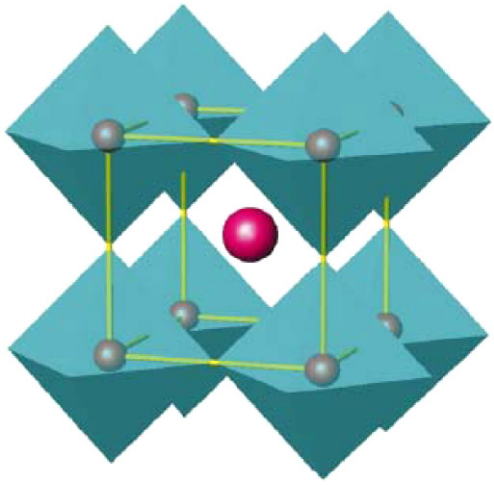

certain $CaTiO_3$-based and complex perovskites with high dielectric constant, low loss and small temperature coefficient of resonant frequency are useful as good dielectric resonator materials for application in microwave frequency range[11,12]. $BiMnO_3$ and $BiFeO_3$ exhibit magnetic and ferroelectric ordering in the same phase giving rise to electric (magnetic) field control of magnetization (polarization). The mutual coupling of the magnetization and polarization imparts additional degree of freedom in the design of actuators, transducers and memory devices. Potential application of magnetoelectric multiferroic includes multi state memory elements[9]. Perovskites are seriously considered for immobilization of high level of radioactive waste produced in nuclear plants[13]. Further, it has been realized that the Earth's lower mantle consists largely of $MgSiO_3$ perovskite. Understanding the behaviour of the silicate perovskite as a function of temperature and pressure is important to appreciate the geophysical properties of the lower mantle and the resulting seismic activities[14,15].

The perovskite structural framework is very flexible and has the capacity to accommodate a variety of foreign cations in its lattice in different degrees. This feature offers a great scope to tailor properties by chemical substitutions. For example Sr substitution for Ba in $BaTiO_3$ not only brings down the Curie temperature near room temperature, but also smears significantly the transition[5]. Both these features are exploited in the fabrication of miniaturized capacitors. It has recently been recognized that the anomalous piezoelectric property of PZT, and other related compounds, arise due to inducement of monoclinic phases in certain composition ranges[16]. Further, the interesting dielectric properties of the structurally non-polar $CaTiO_3$ (CT) and $SrTiO_3$ (ST) arise from the peculiar polar phonon dynamics of these materials[17–19] and their response to different chemical substitutions.

Long ago, in 1957, Kay and Bailey[20] had established that the mineral perovskite, $CaTiO_3$ (CT), possesses orthorhombic structure with space group Pbnm. In fact, except for a countable minority such as $SrTiO_3$ (ST), $BaZrO_3$ (BZ) and $KTaO_3$ (KT), majority of the perovskites exhibit non-cubic structure at room temperature. CT is known to transform to the cubic phase above 1523 K[21]. From the structural point of view, a cubic perovskite structure is the simplest among inorganic compounds with two different cations (A and B). Fig. 1 shows a typical cubic perovskite structure. It consists of corner shared octahedra with the B ions sitting at the centre of the octahedra and the A ions occupying the space between the octahedra. The space group of the cubic perovskite structure is Pm-3m, with all the five atoms occupying the centre of symmetry positions. The structure does not therefore have internal degree of freedom and the only variable is the lattice parameter. The structures of the majority of the perovskites involve cooperative tilting of the anion octahedra about their three tetrad axes. A systematic classification of the various possible tilted octahedral structures is given by Glazer[22,23], who considered the overall distortion in terms of component tilts of the octahedra about the pseudocubic axes, i.e., axes of the parent cubic structure. Due to the constrain imposed by the corner-linked octahedral framework, a clockwise tilt of one of the octahedra about, say [001] axis, would induce an anticlockwise tilt to all four adjacent octahedra perpendicular to the tilt axis. However, there is freedom to all the octahedra along the tilt axis to rotate/tilt about that axis in the same direction (in-phase or + tilt) or opposite direction (out-of-phase or − tilt) with either equal or unequal magnitude. Fig. 2 shows an illustration of an out-of-phase (−) tilted octahedra network. A complete tilt specification of a distorted structure, in the Glazer's notation, is denoted as $a^{\#}b^{\#}c^{\#}$, where the letters a, b and c designate the pseudo-cubic tilt axis, and the superscript can be + or −, depending on whether the adjacent octahedra along that particular tilt axis is rotated in-phase or out-of-phase. In this notation, the equality of two letters implies that the magnitudes of the tilts along those axes are same. A total of 23 different tilt systems have been tabulated

Figure 2: Schematic of a $a^0a^0c^-$ tilted octahedral network. The tilt axis in this diagram is perpendicular to the page.

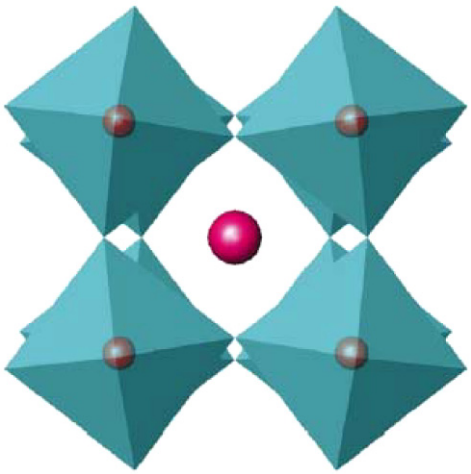

in this manner[23]. Later, group theoretical analysis of this classification scheme by Howard and Stokes[24] predicted only 15 of the 23 tilt systems to be unique. In this formalism, the in-phase (+) and the out-of-phase (−) tilts are associated with irreducible representations (irrep), M_3^+ (k= 1/2, 1/2, 0) and R_4^+ (k = 1/2, 1/2, 1/2), respectively, of the parent cubic structure. These distortions correspond to the M and R points of the cubic Brillouin zone. Because of its generality, the group theoretical treatment can take into account other kinds of distortions not considered in the Glazer's original work and also their coupling. For example, one can consider various types ferroelectric distortions (represented with the irrep Γ_4^-), antiferroelectric distortions, distortions associated with symmetries other than R and M points of the cubic Brillouin zone. Careful analyses of the diffraction patterns of the system, $Sr_{1-x}Ca_xTiO_3$ (SCT), have established an unusual distortion associated with the line symmetry, T ($k = 1/2, 1/2, \xi$), of the cubic Brillouin zone. An uncommon monoclinic structure, resulting from a coupling of a ferroelectric and R-point distortion, was discovered by us in PZT[25–27].

Powder diffraction technique is often the preferred choice for identification of distortions in perovskites. For a cubic perovskite lattice, all Bragg peaks in a powder diffraction pattern must be singlet. For distortions associated with the centre of the cubic Brillouin zone ($k = 0, 0, 0$) (ferrodistortive distortions), the periodicity of the lattice is not affected. The structures resulting from such distortions exhibit powder diffraction patterns that have some or all the cubic peaks split. For example, a tetragonal distortion of the cubic lattice would split the cubic {h00} reflections into two while retaining the singlet appearance of the cubic {hhh}. The reverse is true for a rhombohedral distortion. A distortion of lower symmetry would split all the cubic peaks. If the distortion is associated with an irrep $k \neq (0,0,0)$, multiplication of lattice periodicity also takes place. This leads to appearance of new superlattice reflections, characteristic of the new periodicity. As mentioned above, most perovskites exhibit cell doubling distortions characterized by M_3^+ and R_4^+. The superlattice reflections, in such cases, appear at reciprocal lattice points corresponding to half-integer indices[22,23] which, when indexed with respect to a doubled pseudocubic subcell ($2a_p \times 2b_p \times 2c_p$), acquire indices with at-least one odd integer. The in-phase (+) and out-of-phase (−) tilts are manifested through the presence of two-odd one-even (*ooe*) integer and all-odd (*ooo*) integer superlattice reflections, respectively. A combination of M_3^+ and R_4^+ also results in distortion associated with the X ($k = 1/2, 0, 0$) point of the cubic Brillouin zone, and hence superlattice reflections of the one-odd two-even types are also observed. Based on these arguments the superlattice reflections with *ooe*, *ooo* and *oee* indices are also characterized as M, R and X family of reflections, respectively. It is obvious that, in this indexing scheme, the reflections with all-even indices correspond to the pseudocubic subcell. By, careful analysis of the distortion/splitting of the pseudocubic Bragg profiles, along with the identification of the types of superlattice reflections (M and/or R type), helps in arriving at a reasonably authentic structure in most of the cases[22,23]. Neutron and x-ray powder diffraction studies often complement each other, more particularly when the distortions are very weak. While, the high resolution aspect of a good quality synchrotron x-ray powder diffraction data can resolve better the weak splitting in the pseudocubic reflections, the strong scattering of neutron by oxygen nucleus helps in revealing the superlattice reflections in a more authentic manner. For a given tilted octahedral structure, the relative intensity of superlattice reflections in a x-ray powder diffraction pattern is significantly smaller than in a neutron powder diffraction pattern.

For materials exhibiting polar transitions (ferroelectric or antiferroelectric), input regarding the polar nature should be obtained by carrying out by dielectric and polarization measurements. Such studies sometimes provide motivation for careful examination of powder diffraction data and lead to discovery of features which would otherwise be easily missed in routine examination of powder

patterns. Below, I discuss some perovskite systems investigated by us, specially the ones that exhibit very weak distortions, over the past one decade. Some of the distortions are very unusual and not so commonly found. Neutron powder diffraction data, in conjunction with Rietveld refinement technique, have proved mandatory to reveal the presence of octahedral tilts, as well as in arriving at the most plausible structure in these systems.

2. The $Sr_{1-x}Ca_xTiO_3$ (SCT) System

$SrTiO_3$ (ST), the prototype cubic perovskite structure, has been the model system for studies related with phonon driven structural phase transitions in solids[28]. It has two soft phonon modes: one corresponding to the R-point of the cubic Brillouin zone[29], and another corresponding to the zone centre (Γ) of the cubic Brillouin zone[17]. The soft phonon at the R-point freezes and stabilizes a tetragonal (space group I4/mcm) structure below 105 K. The neighbouring oxygen octahedra along the c-axis of the tetragonal cell are rotated out-of-phase[30], and the structure conforms to the $a^0a^0c^-$ tilt system[22,23]. This transition is non-polar in nature. The zone-center soft transverse optic (TO) phonon continues to soften down to $\sim$ 4 K but does not freeze[31]. The phase below 4 K is called quantum paraelectric state since the quantum fluctuations suppress the onset of an impending ferroelectric phase[8]. The temperature dependence of permittivities of $KTaO_3$[32] and $CaTiO_3$ (CT)[33,34] also follow a similar behaviour.

2.1. *Antiferroelectric phase in the $SrTiO_3$–$CaTiO_3$ (SCT) system*

As mentioned above, both ST and CT show features of quantum paraelectricity at low temperatures. Cowley[17] first reported that ST exhibits a soft transverse optic (TO) phonon, the frequency of which follows Cochran's law, $\omega(TO) \propto (T - T_o)^{1/2}$, and also relates very well to the rise in the relative permittivity in accordance with the Lyddane Sasch Teller (LST) relationship, $\varepsilon(0)/\varepsilon(\infty) = (\omega(LO)/\omega(TO))^2$ [17]. However, instead of freezing, the frequency of the TO mode settles down to a minimum value due to quantum fluctuations and stabilizes a quantum paraelectric state[8]. Since the system is on the verge of a ferroelectric instability, it is highly susceptible to perturbing fields such as uniaxial stress[35], external electric field[36], chemical and isotopic substitutions[37–39], which can induce ferroelectric correlations. As such, ST is also known as an "incipient ferroelectric". Although, in analogy with ST, CT has been described as an "incipient ferroelectric" at low temperatures, so far there has been no evidence of ferroelectricity in pure and doped CT. Lemanov et al have shown that no peak develops in the relative permittivity of 5 mol % of Pb-doped CT, and the quantum paraelectric behaviour persisted at low temperatures[33]. Further, unlike ST, the permittivity is almost insensitive to external electric field up to 40 kV/cm[40]. In view of this, we feel that the use of the term "incipient ferroelectric" in the context of CT is not justified. Our studies on doped CT systems, have led us to speculate that instead of being an incipient ferroelectric, the low temperature phase of CT is more likely to be "incipient antiferroelectric".

Bednorz and Muller (B & M) have shown that Ca substitution in ST ($Sr_{1-x}Ca_xTiO_3$) give rise to sharp peaks in the temperature dependence of the permittivity ($\varepsilon(T)$) plots, for $x < 0.016$[37]. The dielectric anomalies associated with $x < 0.016$ was attributed to quantum ferroelectric phase transitions since the anomaly temperatures (T_m) follow the $(x - x_c)^{1/2}$ dependence. For $0.016 < x \leqslant 0.12$, the peaks smear and the peak value of the relative permittivity decrease continuously with increasing x. Interestingly, T_m remains constant at $\sim$ 35 K for all the compositions in this range. Earlier, Mitsui and Westphal (M & W)[41] had reported peaks in their $\varepsilon(T)$ plots of ceramic SCT specimens with $0.0 \leqslant x \leqslant 0.20$. It is interesting to note that although M & W have reported that dielectric anomalies upto $x = 0.20$, they could observe slim dielectric hysteresis loops, characteristic of ferroelectric correlations, only for $x \leqslant 0.10$. Another interesting observation was the linear increase in T_m with x for $x > 0.12$. B & M had attributed the broadening of the dielectric peaks to random fields due to fraction of Ca^{2+} ions occupying the Ti^{4+} positions resulting in the creation of Ca^{2+}–V_o dipoles. We tested the plausibility of this proposition by Rietveld analysis of neutron powder diffraction data. Ca and Ti have opposite sign of coherent scattering lengths ($b_{Ca} = 4.9$ fm, and $b_{Ti} = -3.44$ fm), and if there is a significant tendency of the Ca to occupy the Ti positions, it would affect the intensities of the Bragg reflections by altering the average scattering length of the B-site. Fortunately, $(1-x)ST-(x)CT$ forms solid solution in the entire composition ($0 \leqslant x \leqslant 1$). Our analysis on $x = 0.25$ and 0.50 suggested that Ca prefers to occupy the Sr site exclusively rather than the Ti site[42]. Thus the proposition of B&M with regard to random fields due to Ca–V_0 centered dipoles does not seem to be plausible. A new explanation was therefore called for, which should not only explain the broadening/smearing of the permittivity peaks but also the absence of ferroelectric correlations for $x > 0.12$, below their respective peak temperatures.

We undertook dielectric studies of $Sr_{1-x}Ca_xTiO_3$ with $x \geqslant 0.18$. Fig. 3 shows

Figure 3: Temperature variation of relative permittivity of $Sr_{1-x}Ca_xTiO_3$ with $0.18 \leqslant x \leqslant 0.40$.

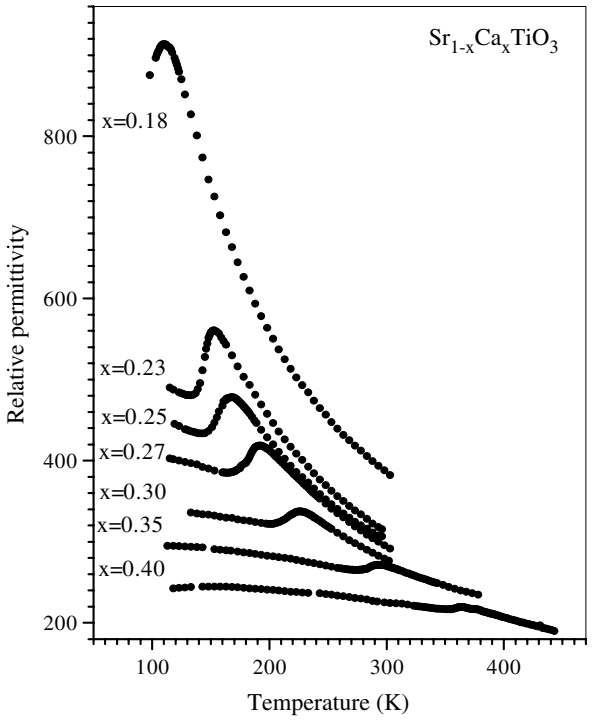

Figure 4: Temperature variation of relative permittivity $Sr_{1-x}Ca_xTiO_3$ with $x = 0.12$, 0.16 and 0.20 (after ref. 41)

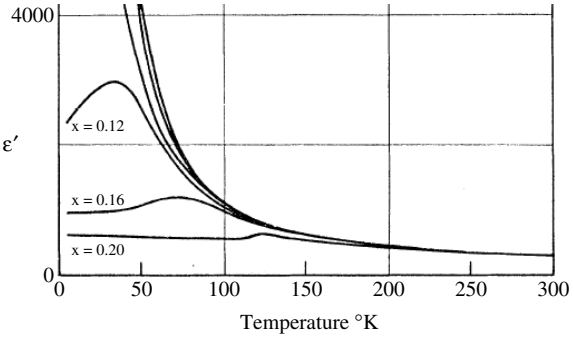

the temperature dependence of relative permittivity, $\varepsilon'(T)$, for compositions in the range $0.18 \leqslant x \leqslant 0.40$[43]. The permittivity peaks apparently appear to be continuation of what has been reported before by B&M[37] and also by M&W[41]. For sake of comparison, a part of the figure showing $\varepsilon\prime$(T) curves has been reproduced from the work of M&W (see Fig. 4). It is noted that the peaks are relatively sharp in Fig. 3 when compared to the peaks corresponding to $x = 0.12$ and 0.16 in Fig. 4. This is more evident in Fig. 5 which shows separately the real (ε') and imaginary (ε'') parts of the relative permittivity of $x = 0.30$. This figure also highlights the fact that $\varepsilon\prime$ and $\varepsilon\prime\prime$ peak at the same temperature suggesting a phase transition[43,44]. The sharpening of the peaks in Fig. 3 suggests that nature of dielectric anomalies have changed for these compositions as compared to $x = 0.12$ and 0.16. The dielectric anomalies have disappeared for $x = 0.43$, as can be seen from Fig. 6, which also shows the $\varepsilon\prime$(T) plot of $x = 0.40$. The inset in this figure shows the magnified plot of $x = 0.40$ near T_m. The sharpness of the $\varepsilon\prime$(T) peak is quite evident for this composition as well.

The polarization–electric field (P–E) hysteresis curves were found to be linear below their respective T_ms behaviour for the compositions shown in Fig. 3. This is in agreement with the observation of M&W who could not see ferroelectric hysteresis loop for $x > 0.10$. A Curie–Weiss analysis of the dielectric data, however, gave negative value of T_0 as shown in Fig. 7 for $x = 0.25$. A negative value of T_0 cannot be explained in terms of the phenomenological theory of ferroelectric transition[1–3]. However, a suitable explanation could be found within the framework of Kittel's phenomenological theory antiferroelectric transition[43,44]. We therefore attributed the dielectric anomalies in Fig. 3 to antiferroelectric (AFE) phase transitions. Intuitively thinking, an antiferroelectric transition is expected to increase of the periodicity of the unit cell of the paraelectric phase. And as such, new superlattice reflections were expected in powder diffraction patterns of the AFE phase. Extensive powder diffraction study was therefore carried out across T_m for some of the compositions in the range $0.18 \leqslant x \leqslant 0.40$. The most readily noticeable change in the powder diffraction pattern across T_m was in the profile shapes of the pseudocubic Bragg reflections. Fig. 8 shows the {400} (or 800 with respect to a doubled cell, $2a_p$ x $2b_p$ x $2c_p$) pseudocubic reflection[45] of $x = 0.30$ on varying the temperature across T_m. The crystal structure of the paraelectric phase has been under controversy. While we proposed an orthorhombic (Ibmm) structure[45], Howard et al[46] showed that the tetragonal structure (I4/mcm) is most likely to be true. The a and b lattice parameter of the tetragonal (I4/mcm) unit cell are 45^0 rotated with respect to two of the pseudocubic axes (a_p and b_p), the tetragonal c-parameter is double the size of the remaining third pseudocubic axis (c_p). With respect the tetragonal (I4/mcm) cell, the splitted peaks are indexed as 008 and 440 (see top panel of Fig. 8). The separation of the 008 and 440 peaks indicates the degree of the tetragonal distortion of the pseudocubic subcell. As temperature decreases,

Figure 5: Temperature variation of real (ε') and imaginary (ε'') parts of relative permittivity of $Sr_{0.7}Ca_{0.3}TiO_3$.

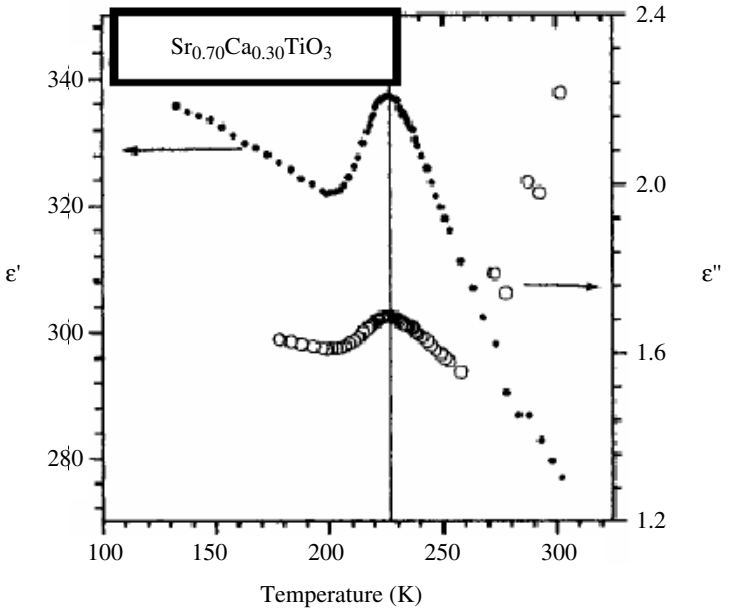

the intensity at the Kα_2 position of the 008 reflection starts increasing below 243 K and that of the 008 reflection decreases concomitantly. At 198 K and below, the 008 reflection has completely vanished. Interestingly, the 440 peak almost seem to remain unaffected. The new peak at the Kα_2 position of the 008 reflection now corresponds to the new c_p pseudocubic subcell parameter of the AFE phase. In fact the pseudocubic Bragg peaks of the AFE phase could be indexed again on the basis of the same tetragonal structure with changed lattice parameters. As can be seen from Fig. 8, the c_p parameter in the AFE phase has decreased sufficiently compared to the paraelectric phase resulting in the near collapse of the tetragonality ($c_p/a_p - 1$) of the pseudocubic cell. This gives the feeling that the pseudocubic subcell of the AFE phase is "nearly cubic". In fact, the phase diagram of M& W mentions "nearly cubic" structures for the lowest temperature phase of $0.12 < x \leqslant 0.20$. This term was also used in the first ever phase diagram of SCT reported by Granicher and Jakits[47]. Fig. 8 also suggests a temperature range (~30 K) in which the structures of the paraelectric and antiferroelectric phases coexist, and also the fact that the new AFE phase emerges gradually from the paraelectric matrix, a phenomena that is akin to martensitic transformation. It may be remarked that during the time of the publication of the results of M & W (in 1961), the accurate structure of low temperature phase of ST was not known, and the term "tetragonal" in the phase diagram of M & W refers to tetragonal distortion of the cubic lattice. The low temperature structure of ST (space group I4/mcm), showing out-of-phase rotation of oxygen octahedra, was solved six years later by Unoki and Sakudo[30].

Although, significant change of the profile shapes of the pseudocubic Bragg reflections clearly reveal the structural phase transition associated with the dielectric anomalies, however, apart from the knowledge about the reduced tetragonality of the pseudocubic axes in the AFE phase, they did not reveal any further information regarding the crystal structure of the AFE phase. A careful examination of the x-ray powder diffraction pattern of the AFE phase led us to identify a new set of very weak superlattice reflections in the powder pattern of the AFE phase. These new reflections are characterized as AFE superlattice reflections. Fig. 9 shows a appropriately magnified powder diffraction pattern of $x = 0.30$ at 300 K (paraelectric phase) and 100 K (antiferroelectric phase)[43,45]. It is evident from this figure that the superlattice reflections, already existing in the paraelectric phase are retained in the AFE phase as well (labeled as S). The pseudocubic reflections are marked as P in this figure. Rietveld analysis of the diffraction pattern of the AFE phase of $x = 0.30$ revealed that a structure type of the paraelectric phase could account for all the S and P peaks but not the AFE peaks. In fact, attempt to index the pattern by le-Bail fit using the lowest symmetry orthorhombic space group P222, which does not have any kind of extinction, failed to index the new AFE reflections. This suggested the need for a new type of supercell to index these peaks accurately. It may be emphasized that if the weak AFE reflections are ignored, the rest of the peaks can be indexed with respect to the cell type (tetragonal, I4/mcm) of the paraelectric phase. The two simplest models to construct a supercell from this tetragonal cell are: (i) by doubling the a-axis (or b-axis) and (ii) by doubling the c-axis. The first model would result in cell type that is known for the antiferroelectric phase of $PbZrO_3$(space group Pbam)[48], whose orthorhombic lattice parameter are related to the pseudocubic lattice parameters as $A_0 \sim \sqrt{2}a_p$, $B_0 \sim 2\sqrt{2}b_p$, $C_0 \sim 2c_p$; the second supercell model gives a cell type that is similar to the antiferroelectric phase of $NaNbO_3$(space group Pbcm)[49] whose orthorhombic lattice (A_0, B_0, C_0) parameters are approximately related to the pseudocubic lattice parameters (a_p, b_p, c_p) as $A_0 \sim \sqrt{2}a_p$, $B_0 \sim \sqrt{2}b_p$, $C_0 \sim 4c_p$. Rietveld refinement was done with both the models. Fig. 10 compares the fits resulting from both the models. It was noted that all the main Bragg peaks

Figure 6: Temperature variation of relative permittivity of $Sr_{0.60}Ca_{0.40}TiO_3$ and $Sr_{0.57}Ca_{0.43}TiO_3$. The inset shows magnified plot of $Sr_{0.60}Ca_{0.40}TiO_3$ near the dielectric peak temperature.

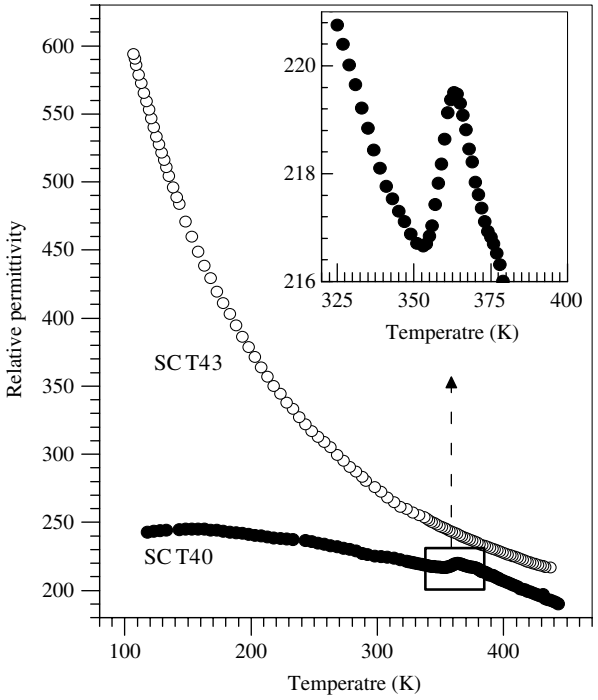

Figure 7: Curie-Weiss fit to the $\varepsilon\prime$(T) data of $Sr_{0.75}Ca_{0.25}TiO_3$.

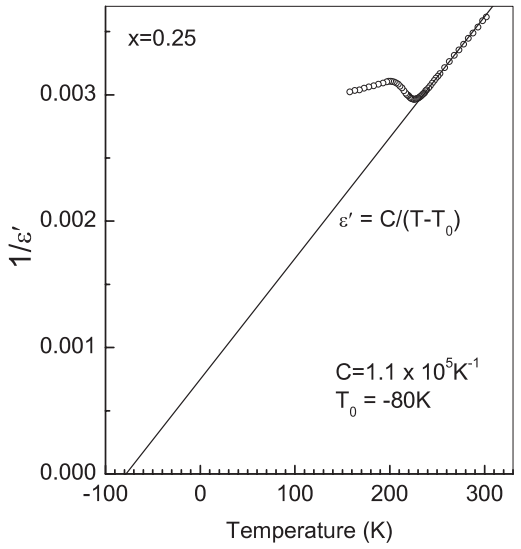

and the superlattice peaks that were retained from the PE phase could be fitted equally well with both the models. A departure of the 0.3 degrees between the peak positions of the observed and the calculated AFE superlattice reflections was observed when fitted with the $PbZrO_3$ structural model[45] (see inset of Fig. 10b). The $NaNbO_3$ (NN) structural model, on the otherhand, fits the peak positions of the AFE reflections very well (see inset of Fig. 10(a)). It was therefore concluded that the AFE structure of the SCT is akin to the antiferroelectric structure of NN. The new AFE superlattice reflections were found for all the compositions exhibiting the AFE transitions, i.e. until $x = 0.40$. For $0.35 < x \leqslant 0.40$, the AFE transition occur above room temperature and as such, the room temperature x-ray powder diffraction patterns of these compositions show the AFE reflections.

2.2. *Structures of SCT at room temperature*

Unaware of the occurrence of AFE phase transition in the compositions range $0.18 \leqslant x \leqslant 0.40$, and the fact that the AFE phase is stable at room temperature for $0.35 < x \leqslant 0.40$, other investigators assumed all the structures in the range $0.40 \leqslant x \leqslant 0.55$ to be orthorhombic Bmmb[50] or Pbnm[51]. Ball et al[50] suggested that structure at room temperature of these compositions is compatible with the space group Bmmb corresponding to $a^0b^-c^+$ tilt system. Perhaps these authors failed to recognize that what appeared as a M superlattice reflection in the room temperature powder diffraction pattern of $x = 0.40$, is in fact a AFE reflection, which could not be indexed on the basis of any of the simple tilted structures proposed in the Glazer's scheme. Further, these authors investigated the SCT system at composition intervals of $\Delta x = 0.05$, and hence any anomalous feature in the diffraction pattern of just one composition, $x = 0.40$, was less likely to attract serious attention. Fig. 11 shows vertically magnified plots of x-ray powder diffraction patterns of selected compositions in the range $0.35 \leqslant x \leqslant 0.43$. The indices are labeled with respect to the doubled pseudocubic cell $2a_p$ x $2b_p$ x $2c_p$. For $x = 0.35$, the superlattice reflections are all of the all-odd, i.e. M type indices and the pattern can be fitted with a tetragonal (I4/mcm) structure consistent with the single out-of-phase tilt system, $a^0a^0c^-$. The patterns of $x = 0.41$ and 0.43 contain both the M and R superlattice reflections. A detailed electron microdiffraction study on a representative composition, $x = 0.50$, proved Pbnm to be the correct space group[52]. The patterns of $x = 0.36$ and 0.40, show a new set of superlattice reflections, marked with arrows, which are not present for $x < 0.36$ and $x > 0.40$. The most unambiguous among these new reflections appears between 56 and 57 degree. The reflection marked with arrow near 37 degree appears very close to the 2θ position of the 310 superlattice reflection, but a careful

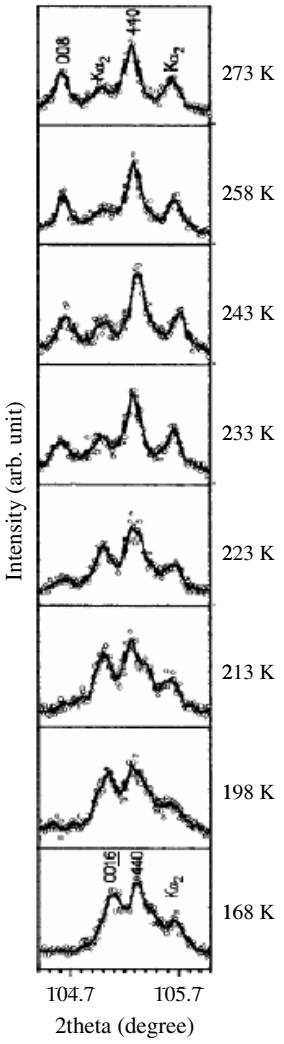

Figure 8: Evolution of the pseudocubic {400} x-ray (Cu Kα radiation) powder diffraction profile of $Sr_{0.70}Ca_{0.30}TiO_3$ with temperature. The indices in the top panel (i.e. at 273 K) are with respect to the tetragonal (I4/mcm) unit cell. The indices in the bottom panel are with respect to the orthorhombic (Pbcm) unit cell (see text). Phase coexistence is clearly evident at 223 K.

examination revealed that the peak positions of the two reflections are distinctly different; the 310 superlattice reflection appears at a lightly lower angle than the AFE reflection. On comparison, it was noted that the positions of the new reflections, are same as that of the AFE reflections of $x = 0.30$. Confirmation of this was done by carrying out Rietveld refinement with three structural models (i) the Bmmb (or Cmcm in a different setting) model, (ii) the Pbnm model, and (iii) the Pbcm model of the AFE phase. The fits shown in Fig. 12 clearly prove that the Pbnm and Bmmb models could not accurately account for the superlattice reflections marked with arrows. The Pbcm model fits the new set of superlattice reflections pretty well. It may be remarked that because of the extremely weak intensities of the new superlattice reflections compared to the other peaks in the pattern, the overall goodness of fit parameters (R-factors and χ^2) was not significantly affected even if the calculated peaks do not account accurately for the observed superlattice peaks in the other models.

More reports in the last two years have confirmed our observation of the new intermediate antiferroelectric phase[53–55]. Very recently, the Howard et al[54] and Anwar & Lalla[55] have carried out detailed electron diffraction studies and have observed superlattice reflections revealing the quadrupling of the periodicity along pseudocubic axis c_p. Analysis of micro-diffraction patterns from a single domain of $Sr_{0.63}Ca_{0.37}TiO_3$ confirmed the Pbcm space group proposed by us. Howard et al[54] showed that the pattern of the superlattice reflections in the electron diffraction patterns for the different zone axes of AFE phase of SCT and $NaNbO_3$ are same. This study therefore gives unambiguous confirmation of the Pbcm space group. The authors also refined the structure of the AFE phase using Rietveld analysis of high quality time-of-flight neutron powder diffraction data collected at 4.2 K. Apart from the R type superlattice reflections arising from R_4^+ (k = 1/2, 1/2, 1/2) distortion of the cubic (Pm3m) structure, these authors reported several other AFE reflections superlattice reflections corresponding to k = 1/2, 1/2, 1/4 and k = 0, 0, 1/4 wave vectors. They correspond to distortions associated with T and Δ points of the cubic Brillouin zone. Analysis of the refined coordinates suggests that the octahedral tilt about the $[\bar{1}10]$ pseudocubic axis, associated with a R_4^+ (k = 1/2, 1/2, 1/2) distortion, is one of the primary distortions of the antiferroelectric structure. The second important primary distortion is the unusual tilt pattern in which two successive octahedra tilt in one sense and the next two in opposite sense leading to doubling of the cell perpendicular to the tilt direction and quadrupling along the tilt direction. This distortion is therefore associated with a T line of symmetry (k = 1/2, 1/2, ξ) with $\xi = 1/4$. It may be noted that $\xi = 1/2$ and 0 are the special points on this line corresponding to R and M points of the Brillouin zone, respectively.

2.3. *Structural distortions and dielectric behaviour of SCT*

It is interesting to note that the onset of the M_3^+ distortion, as manifested by the M superlattice reflections in the room temperature diffraction

Figure 9: Magnified x-ray (Cu Kα radiation) powder diffraction patterns of $Sr_{0.70}Ca_{0.30}TiO_3$ at (a) 300 K (paraelectric phase) and (b) 100 K (antiferroelectric phase). The intensity scale is normalized with respect to the counts of the highest peak in each pattern to emphasize the weak relative intensities of the superlattice reflections. The P and S correspond to the pseudocubic and superlattice reflections. The antiferroelectric reflections are marked as AFE.

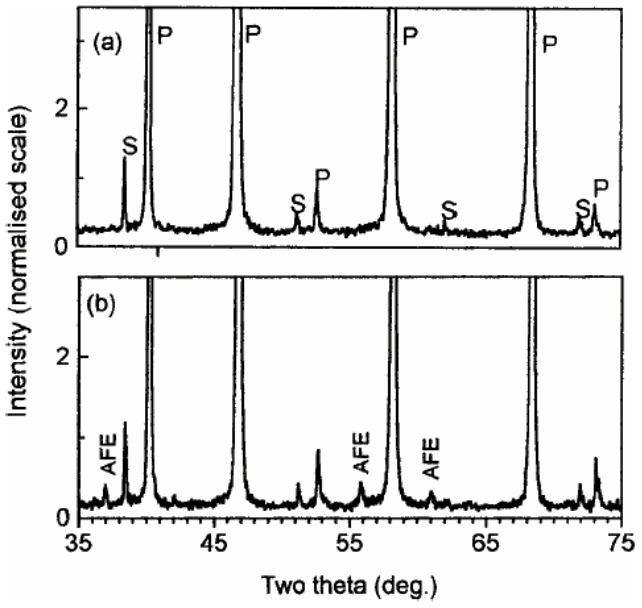

Figure 10: Observed (open circles) and calculated (continuous lines) x-ray (Cu Kα radiation) powder diffraction patterns of $Sr_{0.70}Ca_{0.30}TiO_3$. The calculated pattern is based on the $NaNbO_3$ structural model in (a) and $PbZrO_3$ type structural model in (b). The difference pattern is shown at the bottom of each plots.

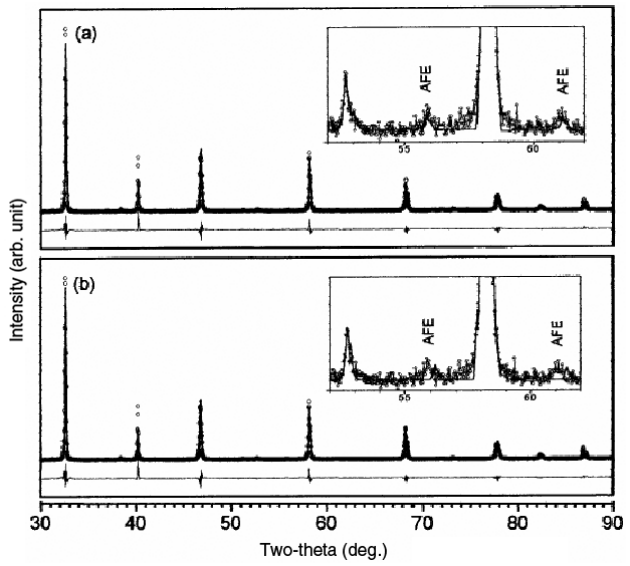

pattern of $x = 0.43$, has significant effect on the dielectric behaviour of the SCT system. As can be seen from Fig. 6, the temperature variation of the relative permittivity of $x = 0.43$ does not show any anomaly upto 450 K, and the relative permittivity increases much sharply at low temperature compared to the neighbouring composition $x = 0.40$. However, similar to $x = 0.40$, the composition $x = 0.43$, exhibits a structural phase transition above 423 K as can be seen from the substantial change of the profile shape (Fig. 13). The M type superlattice reflections vanishes at 500 K, suggesting that this transition is associated with vanishing of the M_3^+ distortion in the orthorhombic Pbnm structure[56]. The high temperature structure is therefore tetragonal (I4/mcm). It is interesting to note that the temperature evolution of the pseudocubic profiles of $x = 0.43$ follows the same trend as in the case of $x = 0.30$ across the AFE phase transition (see Fig. 8), and variation of pseudocubic lattice parameters (a_p, b_p, c_p) with temperature of $x = 0.43$ (shown in Fig. 14) and $x = 0.40$ (Fig. 15) are remarkably identical. For sake of comparison we also carried out powder diffraction study as a function of temperature of $x = 0.12$, which exhibits a smeared dielectric anomaly at T_m = 35 K (see Fig. 4). However unlike the compositions $0.18 \leqslant x \leqslant 0.40$, no sign of appearance/disappearance of peaks in the entire temperature range could be observed down to 12 K. The tetragonality ($c_p/a_p - 1$) of the pseudocubic subcell increases on cooling until ~50 K and then shows a slight decrease (Fig. 16). This clearly demonstrated that the smeared dielectric anomaly ($T_m \sim 35$ K) of $x = 0.12$ is not associated with a structural phase transition.

The cubic (Pm3m)-tetragonal (I4/mcm) phase transition is common to all the compositions in the SCT system. The issue of significance is the role of composition in further activation of distortion in the tetragonal (I4/mcm) phase on the lowering of temperature. It is obvious from the results discussed above that for $x < 0.15$, no further distortion could nucleate in the tetragonal (I4/mcm) phase on cooling down to the lowest temperature; the ground state structure remains tetragonal (I4/mcm). Such compositions exhibit increasingly smeared anomalies with increasing x. For $0.18 \leqslant x \leqslant 0.40$ a distortion associated with a point (k = 1/2, 1/2, 1/4) on the T line of symmetry (of the cubic Brillouin zone) is able to nucleate in the tetragonal phase, leading to stabilization of a $NaNbO_3$ type orthorhombic (Pbcm) as the ground state structure. On further increasing the concentration beyond $x = 0.40$, the M_3^+ distortion wins over the T (k = 1/2, 1/2, 1/4) distortion and precludes the AFE (Pbcm) phase. The ground state for these compositions

Figure 11: X-ray (Cu Kα radiation) powder diffraction pattern of $Sr_{1-x}Ca_xTiO_3$ ($x = 0.35$, 0.36, 0.40, 0.41 and 0.43) at room temperature. The indices are labeled with respect to a doubled pseudocubic cell ($2a_p$ x $2b_p$ x $2c_p$). The M (odd-odd-even) and R (odd-odd-odd) reflections correspond to in-phase and out-of-phase tilts, respectively. The AFE reflections are marked with arrows.

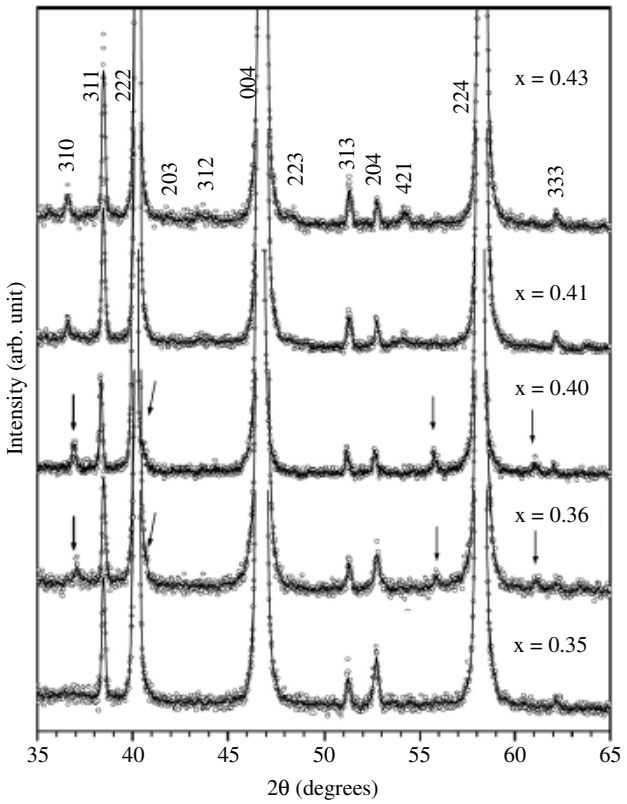

is $CaTiO_3$ type orthorhombic (Pbnm) structure. Interestingly, these compositions seem to exhibit the quantum paraelectric behaviour at low temperature. It is, therefore, tempting to argue that the rising permittivity on cooling CT is manifestation of an incipient antiferroelectric behaviour rather than incipient ferroelectric behaviour suggested by the previous workers[33,34].

2.4. *Competing instabilities in ST–CT system*

Having discovered the AFE phase transition in the SCT system, we are in a position to argue about the smeared dielectric anomalies of SCT reported by B&M and M&W. We have seen in the previous section that the dielectric anomaly of $x = 0.12$ is not associated with structural phase transition. The broad peaks of $x = 0.12$ and 0.16, in Fig. 4, are therefore suggestive of what was earlier known in the literatures of mixed ferroelectric systems as "diffuse transition". Most of the diffuse transitions were later found to be representative feature of relaxor ferroelectric or dipole glass behaviour[32]. The permittivity peaks in such systems arise from relaxation of the localized polar nano regions (PNRs) under the influence of oscillating weak electric field, and do not signal a structural phase transition. The dielectric studies on SCT have so far been focused on dilute Ca doped systems, and detailed dielectric study of the broad peaks exhibited by the compositions $0.06 < x < 0.18$ is still lacking. It is therefore still not clear if the broad peaks exhibit dielectric relaxation or not. M&W[41] have however noted that the system shows slim dielectric hysteresis loop characteristic of a relaxor ferroelectric for $x \leqslant 0.10$. The loops were reported to vanish for $x > 0.10$ despite the continuation of the dielectric anomalies for compositions $x > 0.10$. This implies that, although dilute concentrations of Ca ($x < 0.016$) could trigger ferroelectric correlations in the otherwise incipient ferroelectric ST, its further increase in concentration tends to suppress the development of that very ferroelectric state. We can understand this phenomenon when we look at the dielectric behaviour from higher Ca concentration side. Since the compositions $0.18 \leqslant x \leqslant 0.40$ stabilize a global antiferroelectric phase, it can be expected that the instability that drives the system towards the AFE phase are operative in, for example, $x = 0.12$ and 0.15 as well. However they are not strong enough to stabilize the AFE phase. On decreasing the Ca concentration further, the ferroelectric correlations start asserting and dielectric hysteresis loops become visible. We therefore argue that broad dielectric peaks represent a situation of competing ferroelectric and antiferroelectric instabilities in this system. In analogy with the relaxor ferroelectric systems exhibiting diffuse transitions, the absence of dielectric hysteresis for $0.10 \leqslant x \leqslant 0.15$ suggest that the broad peaks of these compositions represent "diffuse antiferroelectric" transition. A cartoon (Fig. 17) tries to capture the essence of what has been stated.

3. Superlattice phase at low temperatures in a MPB composition of PZT

The high performance piezoelectric ceramics, lead-zirconate-titanate (PZT) ceramics, a solid solution of $PbZrO_3$ and $PbTiO_3$ ($PbZr_{1-x}Ti_xO_3$), is the basis of most electromechanical devices in sonars, hydrophones, micropositioners, high voltage generators, etc[3,4]. The high piezoelectric coefficients occur for compositions close to the boundary separating the tetragonal and rhombohedral phases in the phase diagram. This boundary has been traditionally known as morphotropic phase boundary (MPB) and occurs at $x \sim 0.5$[5]. The direction of spontaneous polarizations in

Figure 12: Observed (dots) and calculated (continuous line) x-ray (Cu Kα radiation) powder diffraction patterns of $Sr_{0.60}Ca_{0.40}TiO_3$. The calculated patterns in (a), (b) and (c) are based on Pbnm, Cmcm and Pbcm structural models (see text). The arrows indicate the positions of the AFE reflections. The vertical bars indicate the calculated positions of the Bragg reflections in each case. Note that the calculated peak positions miss the observed AFE peaks in (a) and (b) but account exactly in (c).

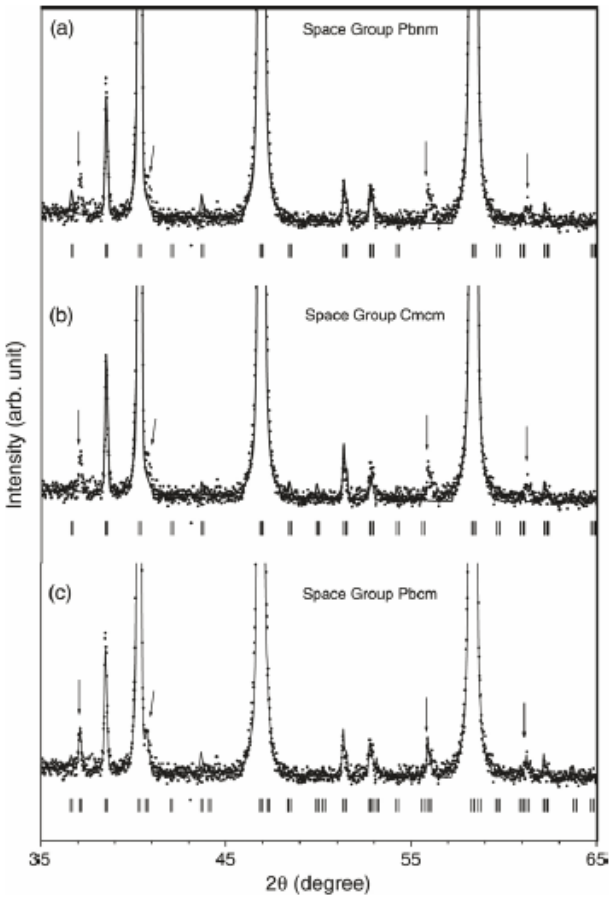

Figure 13: Evolution of the pseudocubic {400} x-ray (Cu Kα radiation) powder diffraction profile of $Sr_{0.57}Ca_{0.43}TiO_3$ with temperature. The indices in the upper panel (i.e. at 573 K) are with respect to the tetragonal (I4/mcm) unit cell. The indices in the bottom panel are with respect to the orthorhombic (Pbnm) unit cell (see text). Phase coexistence is clearly evident at 463 K. Note the similarity in the collapse of the tetragonality of the pseudocubic subcell in the Pbnm phase of this composition and that of the Pbcm phase of $Sr_{0.60}Ca_{0.40}TiO_3$.

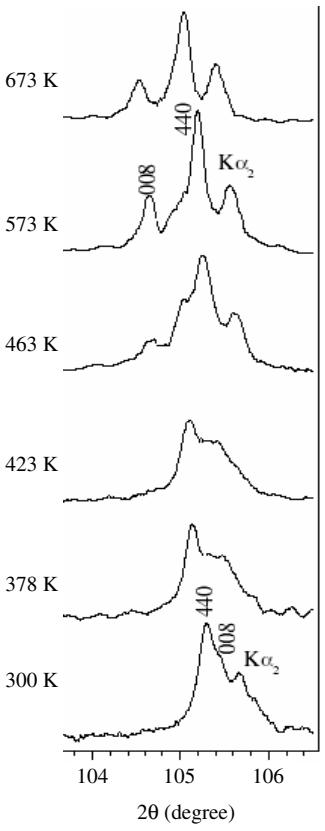

the rhombohedral and tetragonal phases are along <111> and <001> pseudocubic cell. A lot of work has been done to understand the nature of MPB and its relation to the large electromechanical properties[16]. A breakthrough in the understanding however started when Du et al[57], using a phenomenological approach, reported that a rhombohedral PZT, whose spontaneous polarization is aligned along <111> direction of the pseudocubic axis, exhibit very large piezoelectric response when field is applied along the tetragonal polar direction [001]. Around the same time Noheda et al[58] reported a monoclinic phase, with space group Cm, at $\sim$ 20 K for the MPB composition of PZT. The authors used high resolution synchrotron x-ray powder diffraction data to arrive at this conclusion. The monoclinic lattice parameters a_m and b_m lie along the face diagonal of the tetragonal base (a–b plane); c_m is nearly equal to the tetragonal c-parameter but slightly tilted away from it. This discovery provided a mechanism to explain the giant piezoelectric response in PZT. The monoclinic phase is considered to provide a bridge between the tetragonal and rhombohedral phases through the common mirror plane m. The polarization vector can easily rotate on the application of external electric field, within the mirror plane of the monoclinic phase, to give giant piezoelectric effect. The original phase diagram given by Jaffe et al[5] was therefore modified to account for the new development[16]. Around the same time, Ragini et al[59] reported two anomalies in physical properties at $\sim$ 210 K and 265 K for the same composition suggesting two transitions below room temperature.

Figure 14: Variation of the pseudocubic subcell parameters (a_p, b_p, c_p) of $Sr_{0.57}Ca_{0.43}TiO_3$ with temperature. These values were obtained from the refined lattice parameters of the structures in the different phases. In the Pbnm phase a_p, b_p, c_p were obtained from the refined orthorhombic lattice parameters (A_o, B_o, C_o) as $a_p = A_o/\sqrt{2}$, $b_p = B_o/\sqrt{2}$ and $c_p = 2C_o$. The tetragonal (I4/mcm) lattice parameters are also related in the same way.

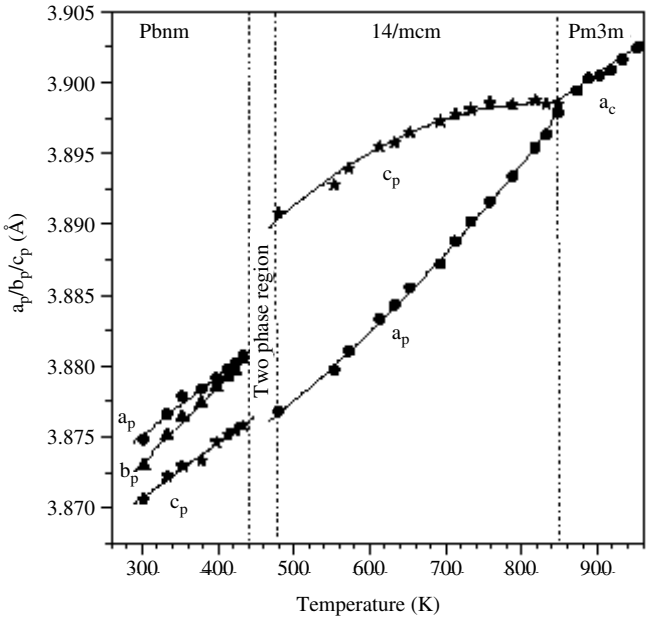

In view of the low temperature monoclinic phase shown by Noheda et al at 20 K, only one transition (P4mm-Cm) was, however, expected below room temperature. What then is the second transition? Ragini et al also reported very weak superlattice reflections in the [101] zone axis electron diffraction patterns at 189 K for a neighboring composition $x = 0.485$. Such superlattice reflections are indicative of cell doubling transition in perovskites and could not be accounted for by the Cm monoclinic cell suggested by Noheda et al[58]. Ragini et al therefore predicted a superlattice phase for the MPB compositions of PZT and attributed the second low temperature anomaly in their physical property measurements to a cell doubling transition. Further confirmation of the existence of superlattice phase at low temperatures came through a detailed temperature dependent neutron powder diffraction study of the MPB composition of PZT[60,61]. Fig. 18 shows very weak, almost invisible, superlattice reflections in the neutron diffraction pattern at 10 K. These reflections are marked with arrows and have been indexed on the basis of a doubled pseudocubic subcell. The all-odd index (R type) superlattice reflections confirms the setting in of R_4^+ ($k = 1/2, 1/2, 1/2$) distortion in the ferroelectric phase of PZT. The appearance of this phase almost coincides with the temperature of second anomaly (~210 K) (see inset (a) of Fig. 18) reported by Ragini et al in their physical property measurements[25]. The intensity of the superlattice reflection increases on cooling down to 10 K implying increasing distortion of the structure. It may be remarked that Noheda et al[58] could not see these reflections in their high resolution x-ray powder diffraction data at 20 K collected at the Brookhaven synchrotron source. This is understandable since the distortions is extremely weak and involve, primarily, displacement of the oxygen atoms which scatter weakly the x-ray radiation. Since, in the absence of the superlattice reflections, the refinement was successful with the Cm structural model, it was clear that the structure obtained at 20 K using the synchrotron data could account for important features of the actual structure. We therefore considered superposing a simple out-of-phase octahedral tilt to the Cm structure reported by Noheda et al. A schematic diagram of this concept is depicted in Fig. 19. The model construction for the superlattice phase was done as follows: (i) two Cm cells are stacked on top of each other along the [001] direction; and (ii) the four equatorial oxygen atoms in the upper and lower cells were rotated out-of-phase[25]. The resulting monoclinic space group was correctly identified as Cc[26]. In fact the group theoretical approach developed by Hatch and Stokes[60] leads to the same space group when a ferroelectric mode associated with a Γ_4^- distortion with polarization components (a, a, b) is coupled to a R_4^+ distortion[26]. Although a single tilt system $a^0a^0c^-$ along the c-direction of the Cm phase, as initially proposed by us, is sufficient to reduce the symmetry to Cc, but the Cc space group also allows tilts in the a–b plane to appear. The generalized tilt-system compatible with the Cc space group is therefore $a^-a^-c^-$. The Cc model could successfully account for the entire neutron powder diffraction pattern at 10 K as shown in the insets (c) and (d) of Fig. 18. In a more careful analysis, a two phase Cc +Cm model gave more improved fitting. This was however challenged by Frantti et al[61] who suggested a combination of Cm + R3c, instead of Cm + Cc model as the correct model. As shown in Fig. 20, the Cm + Cc model was found to explain the peak positions of the superlattice peak more accurately as compared to Cm + R3c, clearly confirming Cm + Cc as the correct model. The Cc space group of the superlattice phase has been verified independently by separate groups[62–65].

Based on the results of first principles calculations, which shows that the ferroelectric and tilt distortions tend to suppress each other[66], it is expected that the superlattice phase is not conducive for enhancement of the ferroelectric

Figure 15: Variation of the pseudocubic subcell parameters (a_p, b_p, c_p) of $Sr_{0.60}Ca_{0.40}TiO_3$ with temperature. These values were obtained from the refined lattice parameters of the structures in the different phases. In the Pbcm phase a_p, b_p, c_p were obtained from the refined orthorhombic lattice parameters (A_o, B_o, C_o) as $a_p = A_o/\sqrt{2}$, $b_p = B_o/\sqrt{2}$ and $c_p = 4C_o$. The tetragonal (I4/mcm) lattice parameters were calculated the way described in the caption of Fig. 14.

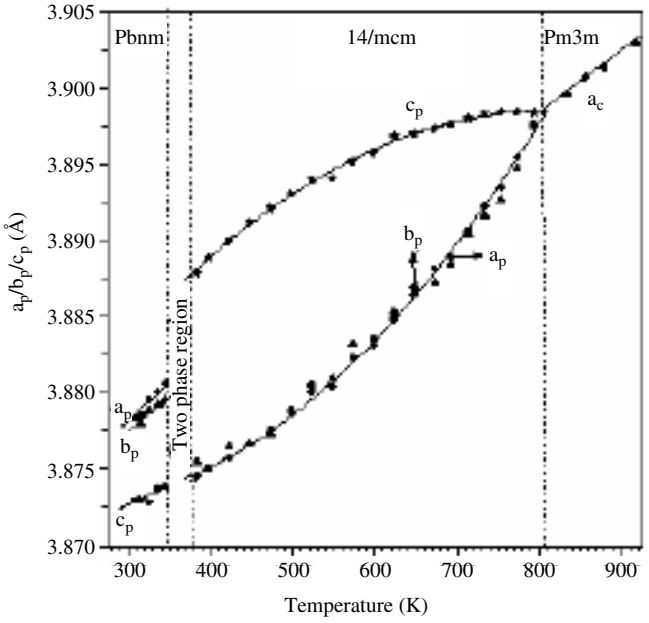

and piezoelectric properties. Grupp et al[67] have shown a decrease of the piezoelectric coefficient of PZT on cooling down to 10 K (see Fig. 3 of ref[67]). It is therefore tempting to attribute the decrease in the piezoelectric coefficients to the stabilization of the superlattice phase and to the increasing rotation angle of the octahedra on cooling. However, a rigorous proof of this argument would require temperature dependent measurement of piezoelectric properties and structure analysis using neutron powder diffraction data on the same batch of specimen.

4. Weak distortions in ($Na_{1/2}$ $Ln_{1/2}$) TiO_3 (Ln=La, Nd, Pr)

Alkali-rare earth complex titanates, $Na_{1/2}Ln_{1/2}TiO_3$ (Ln = La, Pr, Nd, etc.), crystallize in perovskites structures. Of these, $Na_{1/2}La_{1/2}TiO_3$ (NLT) belongs to the Loparite family of minerals found in foidolites and aegirine-albite metasomatic rocks[68]. Apart from the mineralogical importance, NLT also exhibits features of quantum paraelectricity similar to $SrTiO_3$ and $CaTiO_3$[69,70]. $Na_{1/2}Nd_{1/2}TiO_3$ (NNT) and $Na_{1/2}Pr_{1/2}TiO_3$ (NPT) also exhibit a similar dielectric behaviour[70]. Because of their extremely weak distortions, early studies on NLT and NNT reported cubic structures[71,72]. Subsequent studies on NLT by different groups have suggested two different structures. While Sun et al[69] have reported rhombohedral structure in space group $R\bar{3}c$, Mitchell and Chakhmouradian[73], and more recently Knapp and Woodward[74] have reported orthorhombic structure in space group *Pbnm*. All the studies so far were carried out using x-ray powder diffraction data. However, as has been discussed in the context of PZT, it is always desirable to do neutron diffraction study for structure determination when the magnitude of the tilt(s) is very small. Neutron powder diffraction study of this compound was therefore carried out. For the same reason, neutron powder diffraction study was also carried out for NNT and NPT.

Visual inspection of the individual peaks of neutron powder diffraction pattern of NLT revealed no sign of splitting of the pseudocubic Bragg reflections. This suggests that the pseudocubic subcell is almost cubic ($a_p \approx b_p \approx c_p$), which is consistent with the earlier structural analysis of this compound[71]. However, there are signatures of superlattice reflections inset of Fig. 21 shows a 2θ region with a R-superlattice reflection, with doubled pseudocubic index 311, confirming the presence of R_4^+ distortion in the structure. For the orthorhombic (Pbnm) structure proposed by some of the workers, one would have expected a M-superlattice reflection, with double pseudocubic index 310, near $2\theta \sim 37°$. The unambiguous absence of this reflection, in this pattern, at once ruled out the orthorhombic Pbnm structure. We attempted refinement of the structure based on two structural models: (i) rhombohedral ($R\bar{3}c$, $a^-a^-a^-$ tilt system) and (ii) tetragonal structure (I4/mcm, $a^0a^0c^-$ tilt system). In principle, it is possible to distinguish between these two models from diffraction data by inspecting the distortion patterns of the pseudocubic reflections. While a tetragonal distortion of the cubic lattice would split the cubic {*h*00} reflections into two and preserve the singlet nature of {*hhh*}, a rhombohedral distortion of the cubic lattice would do the opposite. However, since all the Bragg peaks were singlet, it was not possible to identify the nature of pseudocubic distortion. Even a high resolution synchrotron data failed to reveal the pseudocubic distortion. We therefore relied on the statistical "goodness of fit" factor (χ^2) to arrive at the most plausible structure of NLT by comparing the fit with tetragonal and rhombohedral structures. The χ^2 obtained after fitting with the rhombohedral and tetragonal structures were 2.91 and 5.56, respectively. We argue that since the statistics of the intensities, particularly the weak superlattice reflections, is very

Figure 16: Temprature variation of the pseudocubic subcell parameters (a_p, b_p, c_p) of $Sr_{0.88}Ca_{0.12}TiO_3$. Contrary to the compositions $x = 0.43$ and 0.40, the tetragonality, as measured in terms of the difference between c_p and a_p does not collapse below the dielectric anomaly temperature (~35 K see Fig. 4). This clearly proves that the dielectric anomaly of $x = 0.12$ is not due to a structural phase transition.

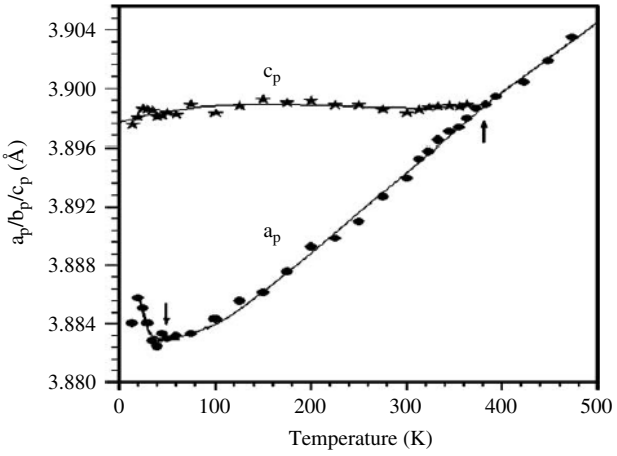

Figure 17: A cartoon illustrating the composition ranges showing ferroelectric, antiferroelectric and competing instabilities in $Sr_{1-x}Ca_xTiO_3$.

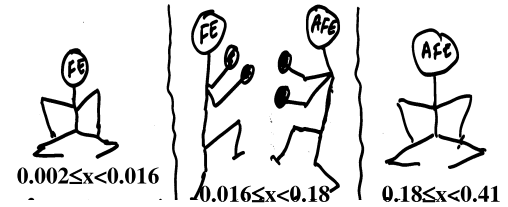

Stable FE	Competing FE and AFE	Stable AFE
Sharp dielectric anomalies	Smeared dielectric anomalies	Sharp dielectric anomalies

good in the present neutron pattern, the difference of 2.7 in the χ^2 values is significant to choose the rhombohedral structure as the most plausible structure[75]. The Rietveld plot after refinement with the rhombohedral structure is shown in Fig. 21.

Similar to NLT, the nature of the distortion of the pseudocubic subcell could not be resolved for NNT and NPT as well. However, in contrast to NLT, the neutron powder diffraction patterns of NPT and NNT contain both the M and R superlattice reflections, confirming the presence of the R_4^+ and M_3^+ distortions (see Fig. 22). A perusal of the various tilt system given by Glazer[22,23] suggests that there are four possible space groups: one in the monoclinic system ($P2_1/m$) and three in the orthorhombic system (Pmmm, Pbnm and Cmcm) which can account for a combination of "+" and "-" tilts. However, because of insignificant distortion of the pseudocubic subcell, we did not consider the low symmetry monoclinic structure. Further, since the intensities of the superlattice reflections corresponding to the "+" tilt are comparatively weaker than those corresponding to the "−" tilt, the space group Pmmm, corresponding to combination of two "+" and one "−" (i.e. + + −), is less likely. We therefore considered only the two remaining space groups, namely Cmcm (or Bmmb in a different setting) and Pbnm. The final choice was based on the comparison of the χ^2 values. It was found that $\chi^2_{Cmcm} = 4.93$ and $\chi^2_{Pbnm} = 3.51$ for NNT, and $\chi^2_{Cmcm} = 3.07$ and $\chi^2_{Pbnm} = 2.50$ for NPT[75]. Although the difference in χ^2 for NPT is not as significantly larger than for NNT, unusual difference in the isotropic displacement parameter for oxygen in 8e and 8f sites was observed when refined in the Cmcm space group. On the other hand, all the isotropic displacement parameters were well behaved for both compounds when refined in the Pbnm space group. We therefore concluded that the structure of NNT and NPT is orthorhombic (Pbnm). In fact, except for NLT, all the structures in the series $Na_{1/2}Ln_{1/2}TiO_3$ are orthorhombic Pbnm[76]. The degree of orthorhombic distortion increases as the Z value of the rare-earth ions increase and even x-ray powder diffraction is good enough to determine the structures reliably.

5. Phase transitions in the system $(1-x)$ $Na_{1/2}$ $Nd_{1/2}$ TiO_3–(x)$SrTiO_3$ (NNT-ST)

Having proved that the structure of NNT is orthorhombic Pbnm ($a^-a^-c^+$ tilt system), we studied how the structure evolved when solid solution of this is compound is formed with the cubic $SrTiO_3$. Fig. 23 shows a limited range of neutron diffraction data of some representative compositions of this series. The indices have been assigned with respect to the doubled pseudocubic cell ($2a_p$x$2b_p$x$2c_p$). Both M and R superlattice reflections are present in the diffraction patterns of the compositions $x = 0.00$, 0.10, 0.20. It was therefore concluded that all these compositions possess the orthorhombic (Pbnm) structure of the parent NNT. For the compositions $x \geqslant 0.30$, the M superlattice reflections disappeared, signaling a structure change. The remaining superlattice reflections are of all-odd type only, indicating presence of only "−" tilt(s) in the structure. A perusal of the possible octahedral distortions given by Howard and Stokes[24] suggests six possible tilt

Figure 18: Neutron (wavelength = 1.667 Å) powder diffraction of $PbZr_{0.52}Ti_{0.48}O_3$ at 10 K. The indices are with respect to a doubled pseudocubic cell ($2a_p$ x $2b_p$ x$2c_p$). The inset (a) shows the appearance. The peak appears at 210 K. Inset (b) shows part of the observed and calculated neutron diffraction pattern after Rietveld refinement with the structural model shown in Fig. 19. Insets (c) and (d) show the magnified plot of (b) near the superlattice reflections [after ref.[25]].

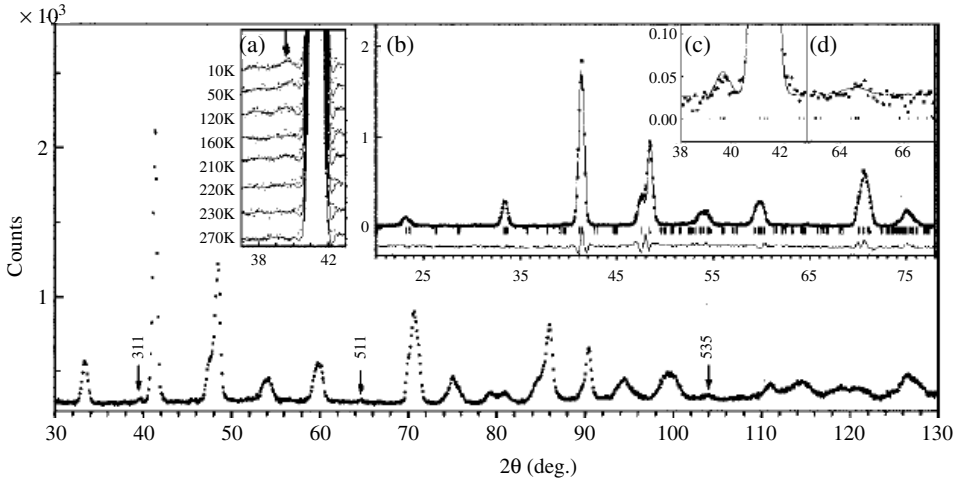

Figure 19: Structural model proposed for the superlattice phase of $PbZr_{0.52}Ti_{0.48}O_3$. It consist of (i) vertical stacking of two Cm type of unit cell proposed by Noheda et al (Ref. 58) and (ii) rotating the four equatorial oxygen atoms in the top and bottom cells in opposite sense (a "−" tilt about the c-axis). The resulting space group is Cc (see text).

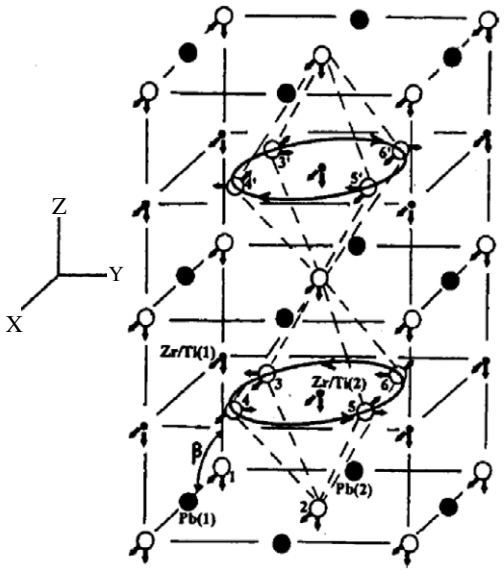

systems with only "−" tilts, namely (i) $a^0a^0c^-$ (tetragonal, I4/mcm), (ii) $a^-a^-a^-$ (rhombohedral, $R\bar{3}2$ c) (iii) $a^0b^-b^-$ (orthorhombic, Imma) or, in a different crystal setting, $a^-a^-c^0$ (Ibmm), (iii) $a^0b^-c^-$ (monoclinic, C2/m), (iv) $a^-b^-b^-$ (monoclinic, C2/c), and (vi) $a^-b^-c^-$ (triclinic, $P\bar{1}$). Our strategy was to consider first the model with highest symmetry and then go for the next lower symmetry and so on. However, unlike for the pure compounds, NLT, NNT and NPT, a signature of splitting was observed in the Bragg reflections some of the NNT-ST compositions. The inset of Fig. 23 shows that the pseudocubic 400 reflection (800 with respect to the doubled cell) is a doublet, suggesting a tetragonal distortion of the pseudocubic lattice of $x = 0.30$. However, the fact that the pseudocubic 004 reflection appear on the higher angle side with respect to its neighbouring 400/040 pseudocubic peak, suggest that the c_p parameter is less than a_p. This is inconsistent with the tetragonal pseudocubic subcell expected on the basis of Glazer's classification scheme which predicts $c_p > a_p$ for the tetragonal (I4/mcm) structure with $a^0a^0c^-$ tilt system[22]. It may, however, be remarked that the I4/mcm space group, as such, does not prevent modelling of an out-of-phase rotation of the neighbouring octahedra along the tetragonal direction even for the case of $c_p < a_p$. The Glazer's scheme is solely based on the natural decrease in the distance between the neighbouring Ti ions on rotation of octahedra about a perpendicular direction. The next possibility was to consider the orthorhombic (Ibmm) structure with $a^-a^-c^0$ tilt system. From the point of view of lattice distortion, this structure can yield pseudo-tetragonal subcell with $c_p < a_p$, and hence this seemed to be most plausible structure for this composition. Rietveld

Figure 20: Selected regions of the observed (dots) and calculated (continuous line) neutron powder diffraction patterns of $PbZr_{0.52}Ti_{0.48}O_3$ at 10 K after Rietveld analysis of the data with pure Cc (top row), Cm+R3c (middle row) and Cc + Cm (bottom row) models. It is obvious from the fits that Cc + Cm result in the best fit of the observed data proving that the superlattice phase is correctly modeled by Cc rather than R3c proposed by Frantti et al (ref. 61) [after ref.[27]]

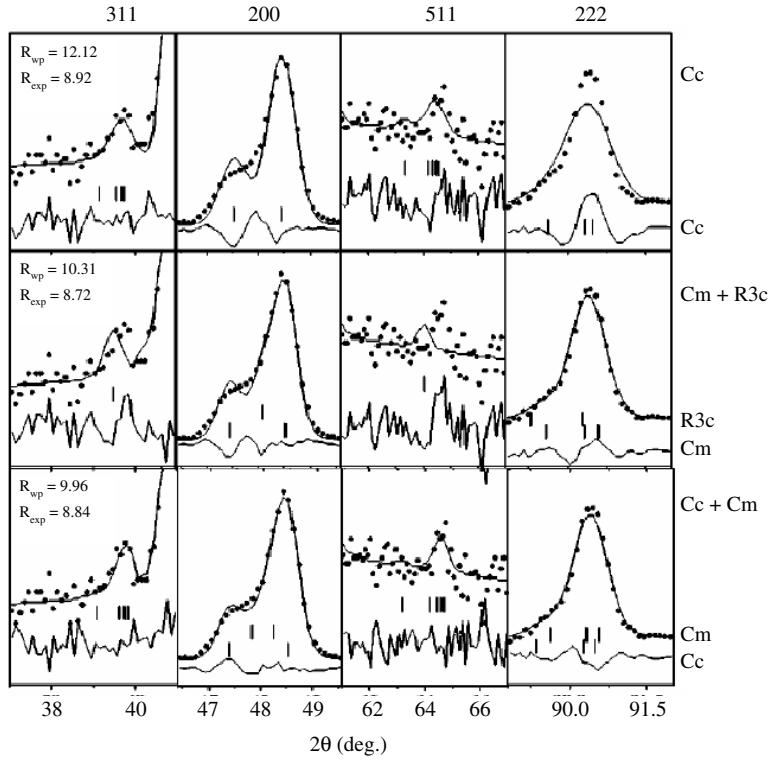

Figure 21: Observed (dots), calculated (continuous line) neutron powder diffraction patterns and difference profiles (bottom of the figure) of $Na_{1/2}La_{1/2}TiO_3$ after refinement with a rhombohedral (R-3c) structure. The inset in the figure highlights the quality of fit of one of the R type superlattice reflections. The data was collected using a neutron wavelength of 1.548 Å [after ref.[75]].

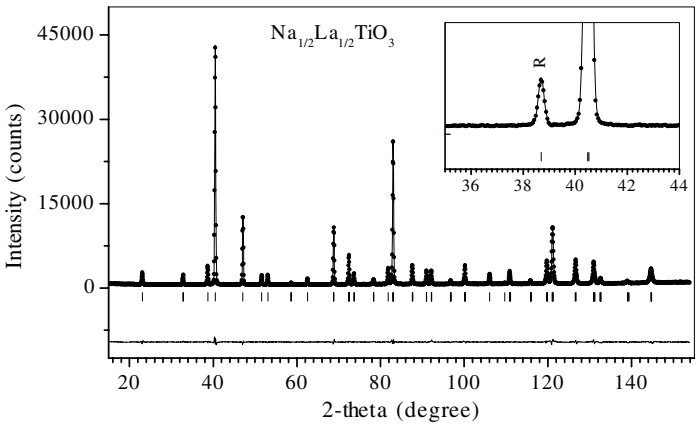

Figure 22: Parts of the neutron powder diffraction pattern of (a) $Na_{1/2}Nd_{1/2}TiO_3$ (NNT) and (b) $Na_{1/2}Pr_{1/2}TiO_3$ (NPT). The indices are with respect to a doubled pseudocubic subcell ($2a_p$ x $2b_p$ x $2c_p$). The M and R superlattice reflections are marked (see text). The data was collected with a neutron wavelength of 1.548 Å [after ref.[76]].

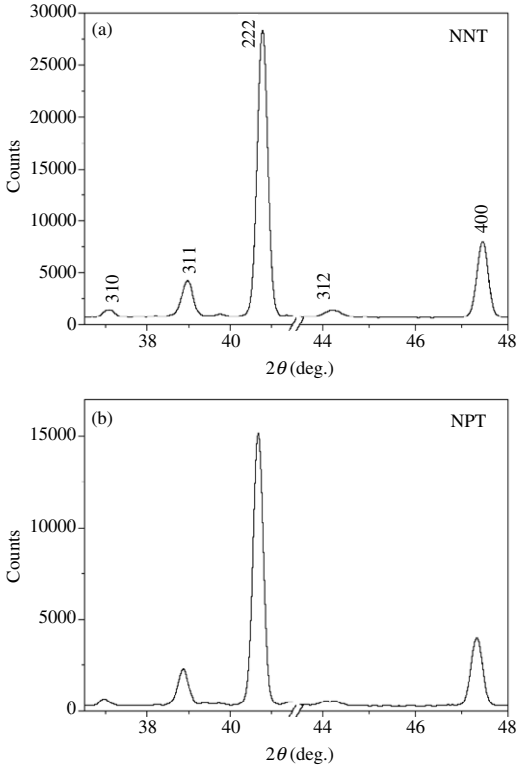

Figure 23: Parts of the neutron (λ = 1.548 Å) powder diffraction patterns of $(1-x)$ $Na_{1/2}Nd_{1/2}TiO_3$-(x)$SrTiO_3$ of selected representative compositions. The indices are with respect to a doubled pseudocubic subcell ($2a_p$ x $2b_p$ x $2c_p$). The inset of $x = 0.30$ shows splitting of the {800} reflection after ref.[77]].

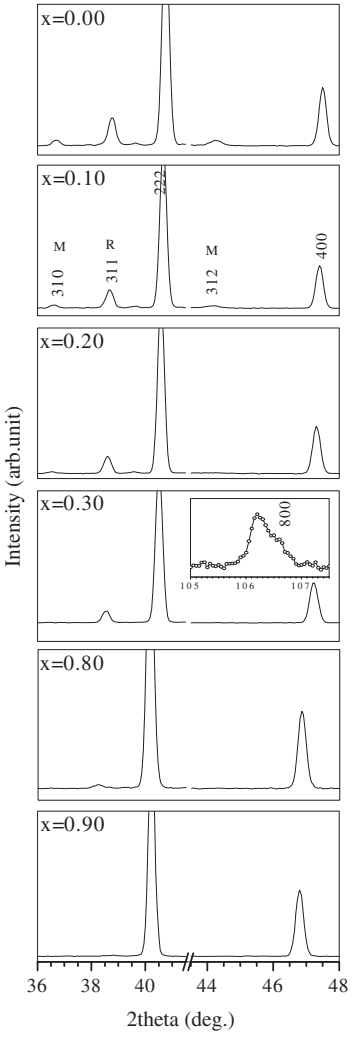

refinement was however carried out with both the models and the results are displayed in Fig. 24. It was possible to distinguish between the better of the I4/mcm and Ibmm structural models only on the basis of fit to the last reflection in the recorded pattern, i.e. near $2\theta \sim 145$[77]. Only the fit with Ibmm structure model could account accurately for this profile (see inset of Fig. 24b). Incidentally, this reflection is a superlattice reflection, and could be seen only in the neutron diffraction pattern and not in xrd pattern due to the form factor consideration. We therefore concluded the structure of $x = 0.30$ as orthorhombic Ibmm. For the neighbouring composition, $x = 0.40$, the same argument was valid. The difference in the quality of fit with the Ibmm and I4/mcm models was not so remarkable for $x \geqslant 0.50$ and the data can be fitted equally well with I4/mcm structure (Fig. 25). It is interesting to note that the relative lengths of the pseudocubic subcell parameters, obtained from the refined lattice parameters, is consistent with the accepted structural models as shown in Fig. 26. For the tetragonal structures c_p is larger than a_p which is consistent with the Glazer's $a^0a^0c^-$ tilt system. The tetragonal (I4/mcm) structure persisted until $x = 0.90$. It is expected that somewhere between $x = 0.90$ and $x = 1.00$ (the $SrTiO_3$ structure), the tetragonal to cubic transition would take place. The sequence of the structural transitions exhibited by this system has also been reported in temperature dependent studies for $SrZrO_3$[78], $SrRuO_3$[79] and in composition studies on the systems

Figure 24: Observed (dots), calculated (continuous line) neutron (λ = 1.548 Å) powder diffraction patterns and difference profiles (bottom of the figure) of 0.70 $Na_{1/2}Nd_{1/2}TiO_3$–0.30$SrTiO_3$ after refinement with (a) tetragonal (I4/mcm) and (b) orthorhombic (Ibmm) structures. The insets in the figures show the fitting of the reflection near 145 degree [after ref.[77]]

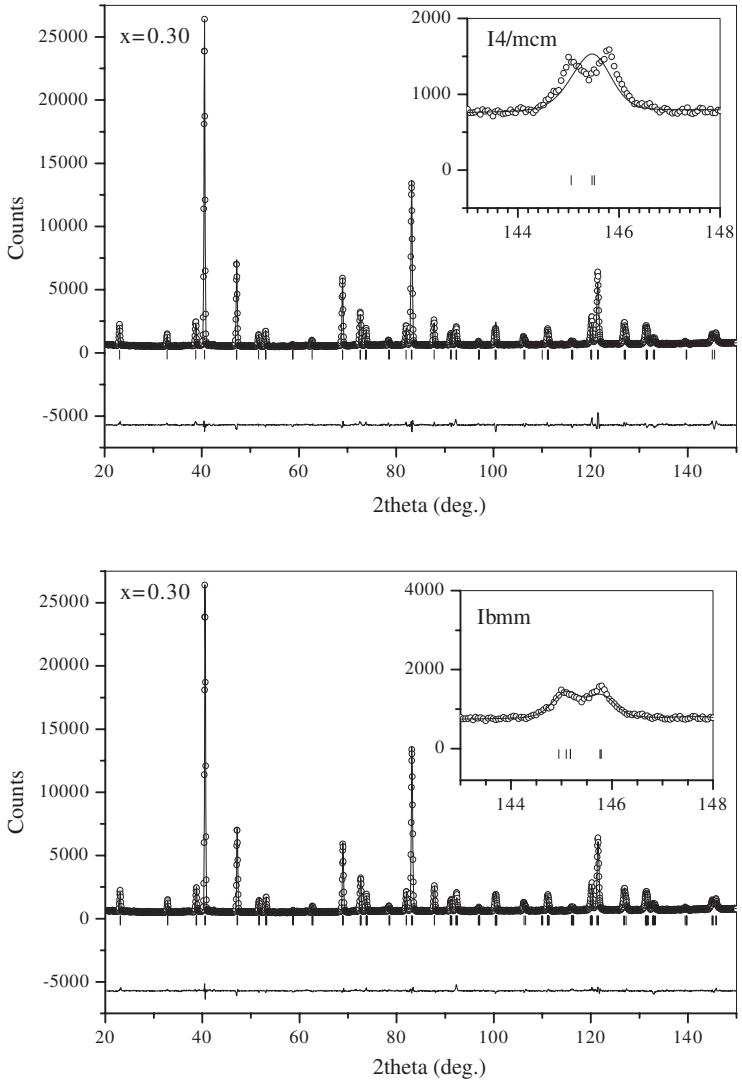

$Sr_{1-x}Ba_xSnO_3$[80] and $Sr_{1-x}Ba_xHfO_3$[81], suggesting that this sequence of transitions is a common feature of many of the orthorhombic perovskites.

It is worthwhile considering the sequence of transitions mentioned above in the light of the symmetry based predictions of Landau theory of phase transitions[24]. As per this analysis, the first transition, i.e., Pbnm–Ibmm, is predicted to be continuous. The same is also true for the Pm3m-I4/mcm transition. However, the Ibmm-I4/mcm transition is predicted to be of discontinuous nature since they are not group-subgroup related. This correlates very well with the discontinuous jumps in the lattice parameters across $0.40 < x < 0.50$. Because of its first order nature, coexistence of the two phases is likely to occur in a certain composition range at room temperature. The features corresponding to the coexistence of Ibmm-I4/mcm may be experimentally difficult to determine using powder diffraction techniques since the set of superlattice reflections are identical for both the Ibmm and I4/mcm structures, and also the fact that the distortions of the subcell from the parent cubic are very weak for both the cases.

6. Structural evidence of quenched ferroelectric nano regions in a Pr-doped $SrTiO_3$

Materials exhibiting ferroelectricity at room temperature and above are technologically very important for device applications[1–5]. As mentioned above, $SrTiO_3$ (ST) is one of the simplest perovskite compounds which has captured the attention of the scientific community for the past four decades, first as a model system for understanding the mechanism of structural phase transitions[3,4], and in recent years because of its incipient ferroelectric behaviour well below 300 K[8,32,33,37–39,82–86]. Attempts have been made to induce ferroelectricity in ST at room temperature. It has been theoretically predicted that biaxial strain can induce ferroelectric state in ST at room temperature and above[87]. The first report in this regard was shown for thin ST film on $DyScO_3$ substrate[88]. Occurrence of epitaxial strain in hetroepitaxial thin films is a natural occurrence, and it can be tuned experimentally. However, application of biaxial strain on bulk specimens cannot be a routine task, and hence inducement of a ferroelectric state at room temperature in bulk ST remained a challenging task. Interestingly, however, Duran et al[89] reported ferroelectricity at room temperature in a Pr doped ST ceramics. This was a bit unusual result, since all the studies in the past have shown that ferroelectric state in doped ST could be induced only well below 300 K. For example, for a Bi-doped ST, it has been shown that polarization survives only upto 100 K[85].

We investigated further the nature of the ferroelectric state in the Pr-doped ST system using dielectric, x-ray powder diffraction, Raman scattering techniques[90,91]. Fig. 27 shows a variation of relative permittivity as a function of temperature at different frequencies on a representative composition, $Sr_{0.95}Pr_{0.05}TiO_3$. The permittivity peak temperature (T_m), increases with increasing frequency. This is manifestation of dielectric relaxation and is one of the important characteristics of relaxor ferroelectrics[92]. The peak temperature, in this case, is not representative of phase

Figure 25: Observed (dots), calculated (continuous line) neutron (λ = 1.548 Å) powder diffraction patterns and difference profiles (bottom of the figure) of 0.50 $Na_{1/2}Nd_{1/2}TiO_3$–0.50$SrTiO_3$ after refinement with tetragonal (I4/mcm) structure. The inset shows a magnified plot near 145 degree [after ref.[77]].

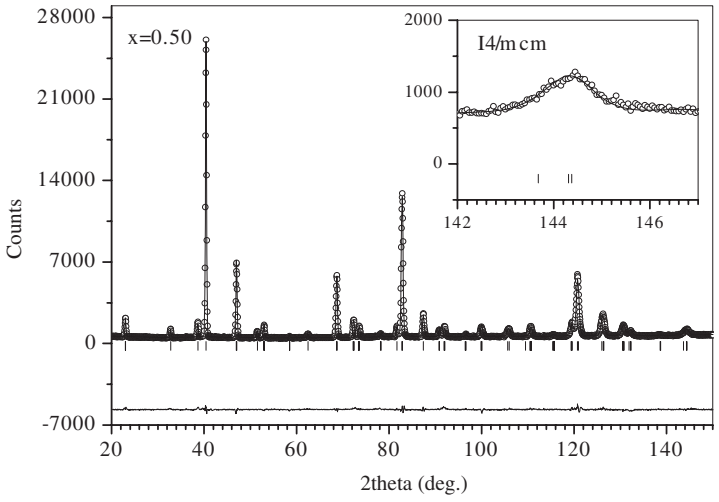

Figure 26: Composition dependence of the pseudocubic lattice parameters (a_p, b_p, c_p) of $(1-x)Na_{1/2}Nd_{1/2}TiO_3$–(x)$SrTiO_3$. Note the abrupt change in the relative magnitude of c_p with respect to a_p/b_p in the composition range $0.40 < x < 0.50$ and its correlation with the change of structure (Ibmm-I4/mcm).

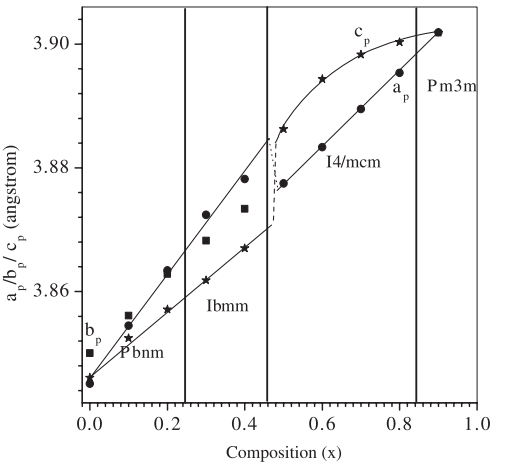

transition but relaxation of dynamic polarized nano regions (PNRs), whose size grow with decreasing temperature. These PNRs may grow sufficiently enough such that they overlap with each other and freeze below T_m to bring about a ferroelectric like state[32]. In perovskites, there are two class of materials which exhibit this phenomena: (i) the dilutely-doped soft ferroelectric mode, incipient ferroelectric systems such as Li and Nb doped $KTaO_3$[93–97] and Ca doped $SrTiO_3$[86], and (ii) the high temperature lead-based strong relaxor ferroelectrics, represented by $Pb(Mg_{1/3}Nb_{2/3})O_3$ (PMN)[92]. It is believed that the soft ferroelectric mode provides the necessary high polarizability to the host lattice, and the electric fields of the local dipoles, formed either due to charge inhomogeneities, as in PMN, or off-centering of the substituted ions as in Ca-doped ST and Li and Nb doped KT, create polarization cloud. The softening tendency of the ferroelectric mode enhances the polarizability of the lattice as it cools and helps the polarization clouds to grow. These clouds are the polarized nano regions (PNRs) mentioned above. What is intriguing in the case of Pr-doped ST is the occurrence of dielectric relaxation around 500 K, a temperature much higher than the conventional dielectric anomaly temperatures in doped incipient ferroelectrics. It may be remarked that this temperature is even higher than the ferroelectric phase transition temperature (130 K) of $BaTiO_3$.

The x-ray powder diffraction pattern of this composition at room temperature revealed all the Bragg peaks to be singlet thereby suggesting a cubic structure (see Fig. 28). Since the room temperature is sufficiently below the permittivity peak temperatures ($\sim$ 500 K), we expect complete freezing of the PNRs at room temperature. By its very nature, a PNR should have a polar non-cubic symmetry. That the xrd pattern shows a globally cubic symmetry can be interpreted in terms of smaller average size of the PNRs as compared to the coherent scattering length of the x-ray beam. A global polar distortion may, however, become noticeable on application of external electric field as in the case of strong relaxors[32,92].

Interestingly enough, the cubic lattice parameter derived from Rietveld fitting of the synchrotron xrd data revealed a strange value: the lattice parameter of $Sr_{0.95}Pr_{0.05}TiO_3$ (3.9052 (1) Å) was same as the standard lattice parameter of $SrTiO_3$ (a = 3.905 Å, Joint Committee on Powder Diffraction Standards (JCPDS) file No. 73-0661). There can be two possibilities: (i) the Pr ions have not entered the lattice of ST, and (ii) The dual valence states of Praseodymium i.e., Pr^{3+} (radius = 1.126 Å)[98] and Pr^{4+} (radius = 0.96 Å)[98], can occupy both Sr^{2+} (radius = 1.44 Å)[98] and Ti^{4+} (radius = 0.61 Å)[98] sites. If parts of the smaller sized Pr^{3+} occupy Sr^{2+}, it would tend to decrease the average volume of the unit cell. This effect can be countered by occupation of parts of the bigger sized Pr^{4+} replacing Ti^{4+}, and preserve the average volume of the unit cell at the value of undoped ST. The first possibility of Pr

Figure 27: (Color online) Temperature variation of real (upper plots) and imaginary parts (lower plots) of the relative dielectric permittivity at various frequencies: (a) 0.4 kHz, (b) 1 kHz, (c) 4 kHz (d) 10 kHz, (e) 40 kHz, and (f) 100 kHz. The arrows indicate the direction of increasing frequency. The inset shows magnified plot of the real and imaginary parts of relative permittivity at 40 kHz [after ref.[90]].

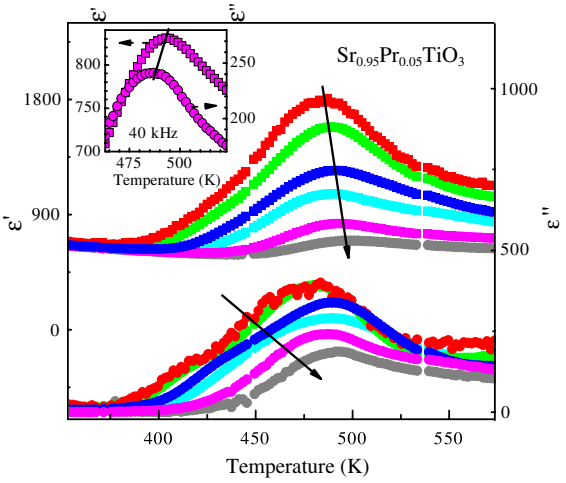

Figure 28: Powder x-ray (λ = 0.79809 Å) diffraction profiles of (a) {111}, (b) {200}, and (c) {220} cubic Bragg reflections of $Sr_{0.95}Pr_{0.05}TiO_3$ [after ref.[90]].

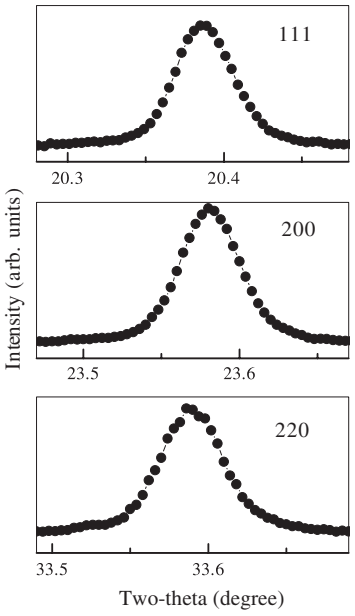

having not entered the ST lattice is ruled out since, we did not notice any feature of impurity peaks in the diffraction pattern. Regarding the second possibility, the issue is debatable since this would require significant fraction of the substituted Pr to replace the Ti. This would raise the question about the displaced Ti, and again, since we did not noticed any impurity peaks in the diffraction pattern the likely hood of this possibility is very insignificant.

We therefore looked for a physical mechanism that might be responsible for this anomalous lattice parameter of $Sr_{0.95}Pr_{0.05}TiO_3$. High temperature diffraction studies were made on $Sr_{0.95}Pr_{0.05}TiO_3$ across T_m to study its thermal expansion behaviour. Fig. 29 shows the variation of lattice parameter with temperature[91]. A distinct change in the slope is clearly visible just above 500 K. The data points above 500 K could be fitted with a linear equation. The observed lattice parameters below 500 K have values larger than that is predicted on the basis of thermal expansion behaviour above 500 K. This graph clearly reveals onset of a spontaneous lattice strain below ~500 K. The anomalies in the lattice expansion and permittivity around 500 K clearly suggests their common origin. Similar spontaneous electrostrictive strains have been reported earlier in high temperature strong relaxor ferroelectric systems such as PMN and La doped lead-zirconate-titanate (PLZT) systems[32]. In these systems, however, the electrostrictive strains start appearing at Burns temperature (T_d) corresponding to the formation of nano-sized polar clusters. T_d is usually more than 100 K above T_m[32]. In contrast, for SPT-05, the onset temperature of electrostrictive strain almost coincides almost with T_m (~500 K). It seems that although SPT-05 shows features of dielectric relaxation, it may be on the verge of exhibiting a ferroelectric phase transition.

For a cubic electrostrictive material, the thermal expansion behaviour is governed by the equation[92]:

$$\frac{\Delta a}{a_0} = \alpha(T - T_0) + (Q_{11} + 2Q_{12})P^2$$
$$= \alpha(T - T_0) + Q_h P^2$$

where a_0 is the reference length at the reference temperature T_0, α is the linear coefficient of thermal expansion, P is the (localized) polarization, and the Qs refer to the various electrostrictive coefficients. On subtracting the pure thermal expansion part from the total expansion of the lattice, one can determine the electrostrictive $Q_h P^2$ contribution to the overall strain. This is shown in the inset of Fig. 29. Since the electrostrictive strain contribution arise from the average local polarization term (P^2), the temperature dependence of the strain, shown in the inset of Fig 5, represents the behaviour of mean-square-polarization with temperature. Interestingly, unlike for the PMN, which shows anomalous strain more than 300 K above its permittivity maximum

Figure 29: Temperature variation of the cubic lattice parameter of $Sr_{0.95}Pr_{0.05}TiO_3$. The straight line is the linear fit to the data points above 500 K. The inset shows evolution of the spontaneous lattice strain with temperature.

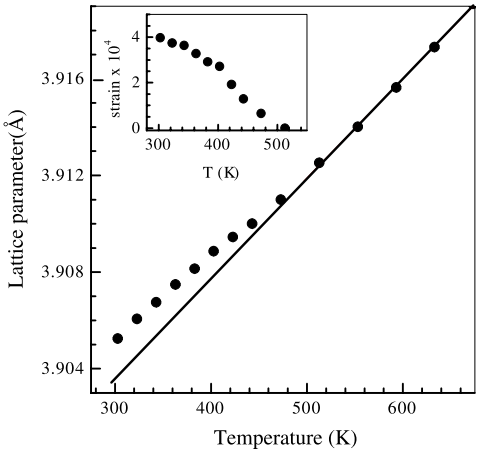

temperature, the electrostrictive strain vanishes just above the permittivity maximum (∼500 K).

This study therefore explains the fact that the anomalous lattice parameter of SPT-05 at room temperature is not merely due to geometrical factors but has significant contribution of electrostrictive strain that spontaneously develops around 500 K due to ferroelectric polar nano regions. In the absence of this phenomenon, the lattice parameter of SPT-05 at room temperature would have been 3.9036 Å, a smaller value, as would be expected due to the smaller sized Pr ions replacing the Sr^{2+} ions in ST. More study is required to understand the exceptional nature of the dipoles in Pr-doped ST. As mentioned above, all studies in the past on doped incipient ferroelectrics have shown ferroelectric state only at cryogenic temperatures. This is due to the fact that polarizability of the host (incipient ferroelectric) increases much faster at temperature sufficiently below room temperature. The PNRs therefore have the opportunity to grow and overlap with each other to bring about a ferroelectric like state at cryogenic temperatures. In view of this, the fact that Pr doping can induce a ferroelectric state at ∼500 K points to the exceptional role of Pr ions in the ST matrix. We propose that Pr defect centers produce giant electric dipoles, the electric fields of which are able to create reasonably large size PNRs which are able to interact and bring about a ferroelectric like state even at such a high temperature. Further investigation is, however, required to understand the peculiar behaviour of this system.

7. Conclusion

Examples of subtle distortions in dielectric and ferroelectric perovskites presented here demonstrate the utility of Rietveld analysis of powder diffraction data in revealing the nature of these distortions. The anomalies in the temperature dependent physical property measurements, such as relative permittivity, polarization and resonance frequency (in case of ferroelectric materials) motivated the search for new phases in SCT and PZT systems. This led to the discovery of an unusual ($NaNbO_3$) type of structural distortion in a certain composition range of the SCT system, missed by other workers, and a new kind of superlattice phase with monoclinic structure in the PZT system. The unique role of neutron powder diffraction method in revealing the subtle distortion associated with the superlattice phase of PZT is clearly demonstrated. Neutron diffraction is shown to be an ideal tool with regard to identification of weak distortions in $Na_{1/2}La_{1/2}TiO_3$, $Na_{1/2}Pr_{1/2}TiO_3$, $Na_{1/2}Nd_{1/2}TiO_3$ and $Na_{1/2}Nd_{1/2}TiO_3$–$SrTiO_3$. The anomalous value of the lattice parameter of a Pr-doped $SrTiO_3$, obtained using Rietveld analysis of high resolution x-ray powder diffraction data helped in discovering spontaneous electrostriction in this material below 500 K which is related to freezing of polar nano regions.

8. Acknowledgment

The author acknowledges the contributions of Professor Dhanajai Pandey, Dr. Sanjay Kumar Mishra, Dr. Akhilesh Kumar Singh and Dr. Hans Boysen, in connection with the research described in this article. Alexander von Humboldt foundation is also gratefully acknowledged for award of research fellowship for carrying out part of the research described in this article.

Received 2 June 2008; revised 5 September 2008.

References

1. Lines, M. E. & Glass, A. M. *Principles and Applications of Ferroelectrics and Related Materials* (Clarendon, Oxford, 1979)
2. F. Jona and G. Shirane, *Ferroelectric Crystals,* (Pergamon Press, 1962)
3. K. Uchino, *Ferroelectric Devices* (Marcel Dekker, Inc, 2000).
4. R. E. Newnham,. Acta Cryst. **A54**, 729, 1998
5. B. Jaffe, W. R. Cook, H. Jaffe, *Piezoelectric Ceramics* (Academic, 1971)
6. A. W. Sleight, J. L.Gillson and P. E.Bierstedt,. Solid State Commun. **17**, 27, 1975
7. J. B Goodenough,. Rep. Prog. Phys. **67**, 1915 (2004).
8. K. A. Muller and H. Burkard Phys. Rev. B **19** 3593, 1979
9. N. A Hill, Annu. Rev. Mater. Res. **32**, 1 2002
10. J. Wang, J. B. Neaton, H. Zheng, V. Nagarajan, S. B. Ogale, B. Liu, D. Viehland, V. Vaithyanathan, D. G. Schlom, U. V. Waghmare, N. A. Spaldin, K. M. Rabe, M. Wuttig, and R. Ramesh, Science **299**, 1719, 2003.

11. S Kawashima, M. Nishida, I. Ueda, and H. Ouchi. J. Am. Ceram. Soc. **66**, 421, 1983
12. S. Kucheiko, J.-W. Choi, H.-J. Kim, and H.-J. Jung, J. Am. Ceram. Soc. **79**, 2739 1996.
13. A.E. Ringwood, S.E. Kesson, K.D. Reeve, D.M. Levins, E.J. Ramm, in: W. Lutze, R.C. Ewing (Eds.), Radioactive Waste Forms for the Future, Elsevier, Amsterdam, 1988, pp. 233–266.
14. R. H. Mitchell. *Perovskites-Modern and Ancient* (Thunder Bay, ON: Almaz Press 2002).
15. M. A. Carpenter, E. K. H. Salje and A. Graeme-Barber. Eur. J. Mineral. **10**, 621, 1998
16. B. Noheda, Curr. Opin. Solid State Mater. Sci. **6** 27 2002
17. R. A. Cowley, Phys. Rev. Lett. **9**, 159, 1962.
18. J. M. Worlock and P. M. Fleury, Phys. Rev. Lett. **19** 1176, 1967
19. E. Cockayne and B. P. Burton, Phys. Rev. B **62** 3735 2000.
20. H. F. Kay & P. C. Bailey, Acta Cryst. **10**, 219, 1957.
21. S. A. T. Redfern, J. Phys.: Condens. Matter **8,** 8267 1996
22. A. M. Glazer Acta Crystallogr. B **28,** 3384, 1972
23. A. M. Glazer Acta Crystallogr. A **31,** 756, 1975
24. C. J. Howard and H. T. Stokes Acta Crystallogr. A **61,** 93, 2005
25. Rajeev Ranjan, Ragini, S. K. Mishra, and Dhananjai Pandey and Brendan J. Kennedy, Phys. Rev. B **65**, 060102(R), 2002
26. D. M. Hatch and H. T. Stokes Rajeev Ranjan, Ragini, S. K. Mishra, and Dhananjai Pandey and Brendan J. Kennedy Phys. Rev. B **65**, 212101, 2002.
27. Rajeev Ranjan, Akhilesh Kumar Singh, Ragini, and Dhananjai Pandey Phys. Rev. B **71**, (2005) 092101
28. A. Bruce and R. Cowley, Adv. Phys. **29**, 219, 1980.
29. P. A. Fleury and J. M. Worlock, Phys. Rev. **174**, 613, 1968.
30. H. Unoki and T. Sakudo, J. Phys. Soc. Japan **23,** 546, 1967.
31. J. M. Worlock and P. A. Fleury, Phys. Rev. Lett. **19,** 1176, 1967
32. G. A. Samara, J. Phys.: Condens. Matter **15**, R367, 2003.
33. V.V. Lemanov, A.V. Sotnikov, E.P. Smirnova, M. Weihnacht, and R. Kunze Solid State Comm. **110,** 611, 1999
34. I. S. Kim, M. Itoh and T. Nakamura, J. Solid State Chem. **101,** 77, 1992
35. H. Uwe and T. Sakudo, Phys. Rev. B **13**, 271, 1976.
36. J Hemberger, O. Lukenheimer, R. Viana, R. Bohmer and A. Loidl Phys. Rev. B**52** 13159 (1995)
37. J. G. Bednorz and K. A. Muller, Phys. Rev. Lett **52,** 2289, 1984
38. V. V. Lemanov, E. P. Smirnova, P. P. Syrnikov and E. A. Tarakanov Phys. Rev. B **54,** 3151, 1996
39. M. Itoh, R. Wang, Y. Inaguma, T. Yamaguchi, Y. –J. Shan, and T. Nakamura, Phys. Rev. Lett. **82**, 3540, 1999.
40. C. Ang, A. S. Bhalla, and L. E. Cross, Phys. Rev. B **64** 184104, 2001
41. T. Mitsui and W. Westphal, Phys. Rev. **124**, 1354, 1961.
42. R. Ranjan, D. Pandey, V. Siruguri, P. S. R. Krishna, and S. K. Paranjpe, J. Phys.: Condens. Matter **11**, 2233, 1999.
43. R. Ranjan, D. Pandey, and N. P. Lalla, Phys. Rev. Lett. **84**, 3726, 2000.
44. R. Ranjan, D. Pandey, J. Phys.: Condens. Matter **13**, 4239, 2001.
45. R. Ranjan, D. Pandey, J. Phys.: Condens. Matter **13** 4251, 2001.
46. C. J. Howard, R L Withers, Z Zhang, K Osaka, K Kato and M Takata, J. Phys.: Condens. Matter **17**, L459, 2005.
47. H. Granicher and O. Jakits, *Suppl*. Nuovo Cimento **9**, 480, 1954.
48. F. Jona, G. Shirane, F. Mazzi and R. Pepinski Phys. Rev. **105,** 849, 1957
49. A. C. Sakowski, K. Lukaszewicz and H. D. Megaw, Acta. Crystallogr. B**25** 851, 1969
50. C. J. Ball, B. D. Begg, D. J Cookson, G. J. Thorogood, and E. R. Vance, J. Solid State Chem. **139**, 238, 1998.
51. T. Yamanaka, N. Hirai and Y. Komatsu, Am. Mineral. **87** 1183, 2002
52. R. Ranjan, D. Pandey, W. Schuddink, O. Richard, P.De. Meulenaere, J. Van Landuyt, G. Tendeloo, J. Solid. State Chem. **162**, 20, 2001.
53. M. A. Carpenter, C. J. Howard, K S Knight and Z Zhang, J. Phys.: Condens. Matter **18**, 10725, 2006.
54. C. J. Howard, R LWithers, K S Knight and Z Zhang, J. Phys.: Condens. Matter **20**, 135202, 2008.
55. S. Anwar and N. P. Lalla, J. Solid State Chem. **181**, 997, 2008.
56. Sanjay Kumar Mishra, Rajeev Ranjan, Dhananjai Pandey, Pierre Ranson, Robert Ouillon, Jean-Paul Pinan-Lucarre and Philippe Pruzan, J. Phys.: Condens. Matter **18,** 1899, 2006.
57. X-H Du, J. Zheng, U Belegundu, K. Uchino, Appl. Phys. Lett. **72,** 2421, 1998.
58. B. Noheda, D. E. Cox, G. Shirane, J. A. Gonzalo, L. E. Cross and S. –E. Park, Appl. Phys. Lett. **74**, 2059, 1999
59. Ragini, S. K. Mishra, D. Pandey, H. Lemmens, and G. Van Tendeloo, Phys. Rev. B **64**, 054101, 2001.
60. D. M. Hatch, H. T. Stokes, and R. M. Putnam,. Phys. Rev. B **35**, 4935, 1987 (also see the implementation of these ideas in the computer Program ISOTROPY , http://stokes.byu.edu/isotropy.html).
61. J. Frantti, S. Ivanov, S. Eriksson, H. Rundolf, V. Lantto, J. Lappalainen, and M. Kakihana, Phys.Rev. B **66,** 064108, 2002.
62. D. E. Cox, B. Noheda, and G. Shirane, Phys. Rev. B **71**, 134110, 2005.
63. B. Noheda, L. Wu, and Y. Zhu, Phys. Rev. B **66**, 060103(R), 2002.
64. J. Rouquette, J. Haines, V. Bornand, M. Pintard, and Ph. Papet W. G. Marshall and S. Hull, Phys. Rev. B **71**, 024112, 2005.
65. David I. Woodward, Jesper Knudsen, and Ian M. Reaney, Phys. Rev. B **72**, 104110, 2005.
66. W. Zhong and D. Vanderbilt, Phys. Rev. Lett. **74,** 2587, 1995
67. D. E. Grupp and A. M. Goldman, Science **1997,** 276, 392.
68. R. H. Mitchell, A.R. Chakhmouradian, P.M. Woodward, Phys. Chem. Minerals **27**, 583, 2000.
69. P. Sun, T. Hsuan, Y. Nakamura, J. Shan, Y. Inaguma, M. Itoh, Ferroelectrics **200**, 93, 1997
70. Y. J. Shan, T. Nakamura, Y. Inaguma, M. Itoh, Solid State Ionics. **108**, 123, 1998.
71. J. Brous, I. Frankuchen, E. Banks, Acta Crystallogr. **6**, 67, 1953.
72. A. Belous, N. Novitskaya, A. Antishko, L. Gavrilova, S. Polyanetskaya and Z. Makarova , Sov. Prog. Chem. **51,** 13, 1985.
73. R. H. Mitchell, R. Chakhmouradian, J. Sol. State Chem. **138**, 307, 1998.
74. M. Knapp, C. Bähtz, H. Ehrenberg, H. Fuess, J. Synchr. Radiat. **11**, 328, 2004.
75. Rajeev Ranjan, Anatoliy Senyshyn, Hans Boysena, Carsten Baehtze, Friedrich Frey, Journal of Solid State Chemistry **180**, 995, 2007.
76. Rajeev Ranjan, Anupriya Agrawal, Anatoliy Senyshyn and Hans Boysen, J. Phys.: Condens. Matter **18,** L515, 2006.
77. Rajeev Ranjan, Anupriya Agrawal, Anatoliy Senyshyn and Hans Boysen, J. Phys.: Condens. Matter **18,** 9679, 2006.
78. C. J. Howard, K. S. Knight, B. J. Kennedy and E. H. Kisi, J. Phys. Condens. Matter **12,** L677, 2000.
79. B. J. Kennedy, B. A. Hunter and J. R. Hester Phys. Rev. B **65,** 224103, 2002
80. E. H. Mountstevens, J. P. Attfield and S. A. T. Redfern J. Phys.: Condens. Matter **15,** 8315, 2003.
81. Li L, Kennedy B J, Kubota Y Kato K and Garrett R F, J. Mater. Chem. **14**, 263, 2004
82. H. C. Li, W. Si, A. D. West, and X. X. Xi, Appl. Phys. Lett. **73**, 190, 1998
83. A. A. Sirenko, I. A. Akimov, J. R. Fox, A. M. Clark, H. Li, W. Si and X. X. Xi, Phys. Rev. Lett. **82**, 4500, 1999.
84. V. Porokhonskyy, A. Pashkin, V. Bovtun, J. Petzelt, M. Savinov, P. Samoukhina, T. Ostapchuk, J. Pokorny, M. Avdeev, A. Kholkin, and P. Vilarinho, Phys. Rev. B **69**, 144104, 2004.
85. C. Ang, Z. Yu, P. Lunkenheimer, J. Hemberger, and A. Loidl, Phys. Rev. B **59**, 6670, 1999
86. U. Bianchi, W. Kleemann, and J. G. Bednorz, J. Phys.: Condens. Matter **6**, 1229, 1994

87. N. A. Pertsev, A. K. Tagantsev, and N. Setter, Phys. Rev. B **61**, R825, 2000
88. J. H. Haeni, P. Irvin, W. Chang, R. Uecker, P. Reiche, Y.L. Li, S. Choudhury, W. Tian, M. E. Hawley, B. Craigo, A. K. Tagantsev, X. Q. Pan, S. K. Streiffer, L. Q. Chen, S. W. Kirchoefer, J. Levy, and D. G. Schlom, Nature **430**, 758, 2004.
89. A. Durán, E. Martínez, J. A. Díaz, and J. M. Siqueiros, J. Appl. Phys. **97**, 104109, 2005.
90. R. Ranjan, R. Hackl, A. Chandra, E. Schmidbauer, D. Trots, Phys. Rev. B, **76**, 224109, 2007
91. R. Ranjan et al, Phys. Rev. B 2008 (in Press)
92. L. E. Cross, Ferroelectrics **76**, 241, 1987
93. P. DiAntonio, B. E. Vugmeister, J. Toulouse, and L. A. Boatner, Phys. Rev. B **47**, 5629, 1993.
94. P. Calvi, P. Camagni, E. Giulotto, and L. Rollandi, Phys. Rev. B **53**, 5240, 1996.
95. J. Toulouse, P. DiAntonio, B. E. Vugmeister, X. M. Wang, and L. A. Knauss, Phys. Rev. Lett. **68**, 232, 1992.
96. R. K. Pattnaik and J. Toulouse, Phys. Rev. B **60**, 7091, 1999.
97. J. Toulouse and R. K. Pattanik, Phys. Rev. B **65**, 024107, 2001
98. R. D. Shannon, Acta Cryst. A, **32**, 75, 1976

Dr. Rajeev Ranjan received his Ph.D from Banaras Hindu University in Materials Science and Technology in 2000. He joined School of Materials Science and Technology, BHU as a lecturer in 2002. He was reader in the same department since 2005 before joining Indian Institute of Science, Bangalore in 2007. He was awarded the Alexander von Humboldt research fellowship during the year 2006–2007 to work on phase transitions in perovskites. His field of research covers several areas such as ferroelectric, piezoelectric, multiferroic materials, magnetic shape memory alloys, and first principles calculations. He has made extensive use of powder diffraction techniques (x-ray and neutron) to investigate structure–property correlations in several interesting oxide perovskites.